Minimal mass and self-stress analysis for innovative V-Expander tensegrity cells

Minimal mass and self-stress analysis for innovative V-Expander tensegrity cells

Aguinaldo Fraddosio[1], Gaetano Pavone[1,*], Mario Daniele Piccioni[1]

[1]*Department of Civil Engineering and Architecture (DICAR), Polytechnic University of Bari, Bari, Italy*

E-mail: *aguinaldo.fraddosio@poliba.it, mariodaniele.piccioni@poliba.it*

E-mail corresponding author: *gaetano.pavone@poliba.it*

Abstract

Tensegrity structures are an intriguing kind of structures by virtue of their deployability, scalability and high stiffness to mass ratio. Fraddosio et al. recently proposed a family of five innovative V-Expander elementary tensegrity cells, characterized by an increasing degree of geometrical complexity, and designed as morphological evolution of a concept originally proposed by Motro and Raducanu. Here, we study the mechanical behavior of these innovative V-Expander elementary tensegrity cells by referring to different topologies; in particular, we analyze for such cells the feasible self-stress states in the cases in which the components in compression are composed of 2, 3, 4 and 6 struts, respectively. In addition, we evaluate the minimal mass of the cells taking into account buckling strength of members in the self-equilibrium states according to the indications of standard building codes.

Keywords

Tensegrity structures; self-equilibrium; minimal mass.

1. Introduction

The term *tensegrity* [1] is a crasis of the two words *tensile* and *integrity* [2]. Such systems have attracted the attention of the researchers in many different fields [3–5] due to their peculiar features and advantages.

From the structural point of view, tensegrity structures are pin-jointed reticulated structures composed of a discontinuous set of component in compression, called struts, inside a continuous tensile network, usually formed by cables or tendons. These structures are capable of being in stable self-equilibrated states in absence of external loads [6]. The process of finding feasible self-equilibrium configurations, that is *form-finding* process or *shape-finding*, is a crucial preliminary step in the design of tensegrity structures. Referring to the definition given in [7], the aim of form-finding process is that of seeking the optimal shape of the structure in a state of static equilibrium.

In recent years many researchers have made considerable efforts in proposing different and efficient form-finding methods, both by means of analytical and numerical approaches [8–13]; for a review of these aspects see [14–17] and references therein.

Analytical methods provide explicit solutions for the self-equilibrium states in which geometrical configurations, connectivity of the elements and mechanical parameters are often defined in a continuous variable form [12]. However, analytical methods are useful and efficient only for small tensegrity structures having marked symmetry properties.

In this work a *form-finding* analysis aimed at determining the feasible self-equilibrium states consistent with an assigned geometrical shape is carried out. In particular we refer to the well-known concept of *force density* [18] within the *Force Density Method* (FDM) [19] (see Section 2 for more details).

In [20], Fraddosio et al. proposed a family of five innovative V-Expander elementary tensegrity cells, characterized by an increasing degree of geometrical complexity, and designed as topological evolutions of a concept originally proposed by Motro and Raducanu [21,22]. The proposed cells are characterized by several advantages, relevant for practical applications: geometrical symmetry, ease of assembly, possibility of deployment and tunability. Moreover, the above-mentioned tensegrity cells, as well as other known tensegrity structures, exhibit a high stiffness to mass ratio. In particular, by using the notation introduced in [23], we denote as V_{kk}-Expander tensegrity cell a structure formed by: two sets of components in compression made of k elements (struts), respectively, each of them connected to one out of the two extremities of the vertical cable (expander axis); a continuous set of both diagonal and horizontal cables.

We further develop the study of the mechanical behaviour of four out of five of the innovative V-Expander elementary tensegrity cells (named Variant I, II, III and IV) introduced in [20]. In particular, for such tensegrity cells we study the feasible self-stress states in the cases in which the components in compression are composed of 2 (topology V_{22}), 3 (topology V_{33}), 4 (topology V_{44}) and 6 struts (topology V_{66}), respectively.

Further goal of the present work is the evaluation of the structural efficiency of the analysed tensegrity cells in terms of minimal mass of the structure in the self-equilibrium states. Structural optimization has been widely studied over the last years: most of these studies focus, for example, on the mass minimization, which is of great technical relevance in structural mechanics, in view of minimization of the cost of the structure [24].

Analyses of the *minimal mass* of the tensegrity structures can be found in [25–28]. Such researches deals with, e.g.: the minimal mass design of tensegrity structures subject to the equilibrium conditions and the maximum stress constraints; the parametric design of tensegrity bridges at different scales of complexity.

Indeed, tensegrity systems can be optimized to reduce the mass and increase the stiffness in virtue of the presence of a number of tensile elements greater than the number of the compressive components [29]. Hence,

recalling that Variant V proposed in [20] has a higher number of struts than that of cables, we do not consider such variant in the following analyses, and we limit the study to Variant I, II, III and IV.

Furthermore, large-scale tensegrity structures can be obtained by means of a suitable assembly of elementary tensegrity cells [30]. Some assembly strategies can be found in [23,31]. In particular, tensegrity grids [32,33], with global and/or local curvature [34,35], as well as tensegrity chains can be assembled by using the innovative V-Expander tensegrity cells. Moreover, research of folding/unfolding and deployment procedures require further studies, with emphasis on the self-stress states and finite mechanisms.

The design of tensegrity structures essentially goes through three stages. Starting from a given configuration, the feasible self-stress states must firstly be determined. Then, the choice of self-stress state having been made, the components must be designed. Finally, analysis of the sensitivity of the system to the inaccuracies in the manufacturing should be carried out [23]. Numerous parameters affect the mechanical behaviour of tensegrity structures: among these, level and distribution of self-stress in the elements and stiffness to mass ratio play a crucial role in the design problem. Knowledge of distribution of the self-stress in a specific geometrical configuration, as well as the minimal masses of the structure in a given feasible self-stress state represent fundamental preliminary data in the design process of tensegrity structures. This study enable us to generalize the mechanical behaviour of the innovative V-Expander tensegrity cells proposed in [20].

The paper is organized as follows. Section 2 gives the theoretical background on the mechanics of tensegrity structures and on the force-finding problem, by means of the approach of the *Force Density Method* (FDM); moreover, it is recalled the classification of self-equilibrium states, and it is introduced the concept of feasible self-equilibrium state. In Section 3 the topology and the morphology for the analysed V-Expander elementary tensegrity cells are described; furthermore, for each Variant (Variant I, II, III and IV) and topology we discuss the kinematic indeterminacy and the static indeterminacy. Section 4 is devoted to the analysis of the feasible self-equilibrium states for each variant and for all the examined topologies. Section 5 deals with the mass minimization problem, studied by applying the design criteria of Eurocode 3: Design of steel structures - Part 1-1: General rules and rules for buildings [36]; in particular, for struts in compression the constraint is represented by the buckling strength, whereas for cables in tension by the yielding strength. The results of the mass minimization problem are presented and discussed in Section 6, where a comparison between all the analysed Variants (Variant I, II, III and IV) and topologies is proposed.

2. Force-finding problem: feasible self-equilibrium states

In order to solve the force-finding problem for a free-standing tensegrity structure we adopt the following assumptions:

- elements (struts and cables) are rectilinear and connected, only at their ends, by pin-joints;
- nodal coordinates and nodal connectivity are given;
- in the self-equilibrium problem no external loads are applied;
- the cross-sectional area A of each element remains unchanged.

In this paper, we consider a tensegrity structure with e elements (which can be partitioned in s struts and c cables, $s + c = e$) connected to n nodes; the nodal coordinates are defined in a Cartesian orthogonal reference system $O\{\mathbf{e}_x, \mathbf{e}_y, \mathbf{e}_z\}$ and are collected in three vectors $\mathbf{x}$, $\mathbf{y}$ and $\mathbf{z} \in \mathbb{R}^n$ whose components are the coordinates in the three directions $\mathbf{e}_x$, $\mathbf{e}_y$, and $\mathbf{e}_z$, respectively.

The topology of the structure, i.e. the connectivity relations between elements and nodes, can be expressed by means of the so-called *Connectivity matrix* $\mathbf{C} \in \mathbb{R}^{exn}$ [19]. If the member k connects node i to node j, then the k-th row of $\mathbf{C}$ has only two non-zero entries in the i-th and j-th position ($i < j$), which are equal to 1 and -1 respectively. Hence:

$$[\mathbf{C}]_{k,p} = \begin{cases} +1 & \text{if } p = i \\ -1 & \text{if } p = j \\ 0 & \text{otherwise} \end{cases} \qquad k = 1,...,e,\ p = 1,...,n. \tag{1}$$

Furthermore, the length l_k of the k-th member can be expressed as:

$$l_k = \sqrt{(x_i - x_j)^2 + (y_i - y_j)^2 + (z_i - z_j)^2}. \tag{2}$$

The self-equilibrium problem can be solved by using the FDM. To this aim, for k-th element of the structure it is possible to determine the force density q_k:

$$q_k = \frac{f_k}{l_k}, \tag{3}$$

where f_k is the internal force in the element k (f_k is positive for cables and negative for struts) in self-stress state. Force densities of the elements can be collected in a diagonal matrix $\mathbf{Q} \in \mathbb{R}^{exe}$, i.e. $\mathbf{Q}=diag\{q_1, q_2,\ldots, q_k\}$; this allows to write the equilibrium equations of the tensegrity structure in the three directions $\mathbf{e}_x$, $\mathbf{e}_y$, and $\mathbf{e}_z$ in the following matrix linear form [15]:

$$\begin{cases} \mathbf{C}^T\mathbf{QCx} = \mathbf{0} \\ \mathbf{C}^T\mathbf{QCy} = \mathbf{0}, \\ \mathbf{C}^T\mathbf{QCz} = \mathbf{0} \end{cases} \tag{4}$$

where the superscript "T" indicates the usual matrix transposition operation. By introducing the *equilibrium matrix* $\mathbf{A} \in \mathbb{R}^{3nxe}$, Eq. (4) can be written in compact form:

$$\mathbf{Aq} = \mathbf{0}, \tag{5}$$

where $\mathbf{q} \in \mathbb{R}^e$ is a vector collecting the elements on the main diagonal of $\mathbf{Q}$ and the equilibrium matrix $\mathbf{A}$ is:

$$\mathbf{A} = \begin{bmatrix} \mathbf{C}^T diag(\mathbf{Cx}) \\ \mathbf{C}^T diag(\mathbf{Cy}) \\ \mathbf{C}^T diag(\mathbf{Cz}) \end{bmatrix}. \tag{6}$$

Notice that Eq. (5) can be directly obtained by a derivation of the force equilibrium conditions on a node of the tensegrity structure [37,38].

It is possible to show that Eq. (6) expresses the relationship between the projected lengths in $\mathbf{e}_x$, $\mathbf{e}_y$, and $\mathbf{e}_z$ directions, respectively, and the force densities of the elements [39]. Let r_A be the rank of $\mathbf{A}$ ($e < 3n$); it is clear from Eq. (5) that if $r_A < e$, non-trivial solutions exist. These non-trivial solutions correspond to n_A *independent self-stress modes*, which can be considered as the bases of the vector space of the force densities of the elements, with:

$$n_A = e - r_A \geq 1. \tag{7}$$

Indeed, the force-finding problem aims at determining the above-introduced n_A bases of the vector space of the force densities of the elements. Moreover, if $r_A < e$, when six rigid-body motions in three-dimensional space are opportunely constrained, the number of possible infinitesimal mechanisms m_i is $m_i = 3n - r_A - 6$ [40]. It follows that tensegrity structures are statically indeterminate and usually kinematically indeterminate structures [41], with $n_A > 1$ and $m_i \geq 0$, respectively.

A general solution $\bar{\mathbf{q}} \in \mathbb{R}^e$ of Eq. (5) can be calculated as linear combination of n_A independent self-stress modes [42], that is:

$$\bar{\mathbf{q}} = \sum_{i=1}^{n_A} \alpha_i \mathbf{q}_i, \tag{8}$$

where α_i, $i = 1, 2, \ldots, n_A$, are the real coefficients of the linear combination. Generally, Eq. (8) leads to an independent self-stress state which is not compatible with the unilateral behavior of the elements, i.e., struts in compression and cables necessarily in tension [43]. Furthermore, for statically indeterminate structures ($n_A \geq 1$) having certain symmetry properties, as is often the case for tensegrity structures, many members are in accordance with the symmetry and then can be collected into suitable groups [44]. An independent self-stress

state consistent with the symmetry properties of the structure is called *integral self-stress mode* $\bar{\mathbf{q}}$, and can be written as:

$$\bar{\mathbf{q}} = \sum_{i=1}^{h} q_i \mathbf{e}_h, \tag{9}$$

where h is the number of the symmetry groups, q_i, $i = 1, 2,\ldots, h$, is the force density of the elements in the i-th group and the vector $\mathbf{e}_i \in \mathbb{R}^e$, $i = 1, 2,\ldots, h$, has non-zero entries, equal to 1, in the i-th position if element i belongs to the same group. Thus, from Eqs. (8) and (9) it is possible to write:

$$\sum_{i=1}^{n_A} \alpha_i \mathbf{q}_i - \sum_{i=1}^{h} q_i \mathbf{e}_h = \mathbf{0}. \tag{10}$$

Let $\bar{\mathbf{S}} \in \mathbb{R}^{ex(n_A+h)}$ be a matrix whose first n_A columns correspond to the independent self-stress modes and the last h columns correspond to the opposite of the above mentioned vectors $\mathbf{e}_i$; then, Eq. (10) leads to:

$$\bar{\mathbf{S}}\boldsymbol{\gamma} = \mathbf{0}, \tag{11}$$

where vector $\boldsymbol{\gamma} \in \mathbb{R}^{(n_A+h)}$ collects the n_A real coefficients of the linear combination in Eq. (8) and the h force densities of the groups in Eq. (9). In this way, it is possible to calculate an integral self-stress state by solving the linear homogenous system in Eq. (11) via Singular Value Decomposition (SVD) [45]. Let $r_{\bar{S}}$ and $n_{\bar{S}}$ be the rank and the dimension of the null space of the matrix $\bar{\mathbf{S}}$, respectively, such that:

$$n_{\bar{S}} = (n_A + h) - r_{\bar{S}}. \tag{12}$$

Then, there exist $n_{\bar{S}}$ independent solutions of Eq. (11). If the rank deficiency $n_{\bar{S}}$ of the matrix $\bar{\mathbf{S}}$ is equal to zero, then the tensegrity structure has not self-equilibrium states consistent with the geometric symmetry. Therefore, $n_{\bar{S}}$ must be greater or equal to 1 in order to ensure the existence of non-trivial solutions of Eq. (11). Here we consider only the case in which $n_{\bar{S}}$ is equal to 1; for $n_{\bar{S}} > 1$ we refer, e.g., to [46].

Finally, *feasible self-stress modes* $\tilde{\mathbf{q}} \in \mathbb{R}^e$ are particular integral self-stress modes satisfying also the unilateral behaviour of the elements (struts only in compression and cables only in tension); a procedure for determining *feasible self-stress modes* is described in [47], to which we refer for full details.

Given a feasible self-stress mode $\tilde{\mathbf{q}}$, the corresponding internal force vector $\tilde{\mathbf{f}} \in \mathbb{R}^e$ can be calculated as:

$$\tilde{\mathbf{f}} = \mathbf{L}\tilde{\mathbf{q}}, \tag{13}$$

where $\mathbf{L} \in \mathbb{R}^{exe}$ is the diagonal matrix whose k-th element of the main diagonal is the length l_k.

3. Topology and morphology of V-Expander tensegrity cells

The study of the topology represents one of the most important step in the analysis of the mechanical behavior of tensegrity structures. In this vein, recently in [48] and [49], innovative methods for topology design of such structures were investigated.

Fraddosio et al. [20] analyzed the properties of a new family of tensegrity cells, which can be viewed also as a possible elementary structures for lattice materials, starting from the original concept of V-Expander tensegrity cells proposed by Motro and Raducanu [50]. In particular, by recalling the definition given by Skelton [6] of a class *k* tensegrity structure as a tensegrity structure that has as many as *k* bars connected at their ends, the original V-Expander can be classified as a class 2 tensegrity structure. In [20] was developed the concept of this innovative cell by means of a topological study, and was proposed five new kind of V-Expander tensegrity cells.

V-Expander tensegrity cells exhibit some intriguing properties and advantages [33]; furthermore, Quirant et al. [51] described a feasible application of the V-Expander tensegrity cells as a constitutive paradigm of a double layer grid.

In this paper we focus our attention on feasible self-stress states of four out of five variants proposed in [20], i.e., Variant I, II, III and IV (Figs. 1-4). In particular, we study some different topologies for each Variant, that is, V_{22}, V_{33}, V_{44}, and V_{66}-Expander elementary cells (Fig. 5). To this aim, we refer to the following three parameters that fully describe the geometry of the cell (Fig. 6):

- r, the radius of the circle circumscribing the quadrangle formed by the nodes of the cell in the xy plane;
- h, the height of the triangle formed by each couple of struts joined by a node of the expander axis;
- d, measures the length of the active cable ($0 < d \leq h$).

Table 1

Static and kinematic determinacy of Variant I

Topology	n	e	c	s	r_A	m_i	n_A
V_{22}	6	11	7	4	10	2	1
V_{33}	8	19	13	6	18	0	1
V_{44}	10	25	17	8	24	0	1
V_{66}	14	37	25	12	36	0	1

Table 2

Static and kinematic determinacy of Variant II

Topology	n	e	c	s	r_A	m_i	n_A
V_{22}	6	12	8	4	11	1	1
V_{33}	8	19	13	6	18	0	1
V_{44}	10	25	17	8	23	1	2
V_{66}	14	37	25	12	35	1	2

Table 3

Static and kinematic determinacy of Variant III

Topology	n	e	c	s	r_A	m_i	n_A
V_{22}	6	13	9	4	12	0	1
V_{33}	8	19	13	6	18	0	1
V_{44}	10	25	17	8	24	0	1
V_{66}	14	37	25	12	36	0	1

For our purposes, it is useful to further define a parameter a equal to the d to h ratio ($0 < a \leq 1$). In order to avoid cell configurations which can lead to potential difficulties in the construction of the cell, we consider a feasibility range for the parameter a, i.e., $0.1 < a \leq 1$ ($a = 0.1$ dot-dashed line in figures); moreover, without loss of generality, we consider for the numerical analyses presented below $r = h = 1000$ mm. Given these assumptions, we determine the force densities (normalized respect to the force density of a set of struts), as well as, the internal forces in the elements as a function of the parameter a.

We show the results of the analysis of the static and kinematic determinacy for the four variants in Tables 1-4. Notice that V_{44}, and V_{66}-Expander tensegrity cells of Variant II and, in addition, all topologies of Variant IV have multiple independent self-stress modes (that is, it results $n_A > 1$). In order to obtain the feasible self-stress states for these tensegrity structures, we calculate the force densities of the elements by applying the procedure described in the previous Section. Notice that the topology V_{22} for both Variant I and II, as well as, the topologies V_{44}, and V_{66} for Variant II, are kinematically indeterminate, i.e., $m_i > 1$, whereas the other examined V-Expander tensegrity topologies are kinematically determinate, i.e., it results $m_i = 0$.

Table 4

Static and kinematic determinacy of Variant IV

Topology	n	e	c	s	r_A	m_i	n_A

V_{22}	6	14	10	4	12	0	2
V_{33}	8	22	16	6	18	0	4
V_{44}	10	29	21	8	24	0	5
V_{66}	14	43	31	12	36	0	7

4. Results: comparison of feasible self-stress states

In this Section we show the results of the analysis of the self-equilibrium problem for all topologies of Variant I, II, III and IV. According to the properties of symmetry of the cells, we compare the values of the force densities and of the internal forces, respectively, for representative elements of the symmetry groups (Fig. 7) and for feasible values of the parameter *a*; in particular we observe how the above-mentioned values change for *a* ranging from 0.1 to 1.

4.1. Variant I

Representative elements of the symmetry groups of Variant I are: vertical, horizontal and diagonal cables; struts. Their force densities can be normalized respect to that of the struts (which, in the present case, assume all the same value).

From Figs. 8, 9 it is clear that V_{22} presents the lowest values of the force densities as well as of the internal forces in the vertical cables among all the examined topologies. In general, we observe that the force densities and the internal forces in these cables increase as the degree of geometrical complexity increases. Moreover, the force densities in such cables decrease with *a* until they reach their minimum in the left neighborhood of $a=1$, while the internal forces in vertical cables are independent of *a*.

The force densities in the horizontal cables increase as the degree of geometrical complexity increases, while decrease as the parameter *a* increases. It is interesting to note that the internal forces in these cables have the same behavior of that of vertical cables; except for the fact that in the horizontal cables for values of the parameter *a* greater than about 0.32 their minimum corresponds to the V_{22} topology; vice versa, for $0.1 < a < 0.32$ the minimal value of the internal forces is attained for V_{33} topology (Figs. 10, 11).

Finally, for what concerns the diagonal cables, their internal forces decrease as the geometrical complexity increases (Fig. 12), while their force densities remain unchanged. Topology V_{22}, for such cables, corresponds to the maximum value of the tensile internal forces.

4.2. Variant II

From the analysis of the feasible self-equilibrium states, it is possible to identify the following elements representative of the symmetry groups of Variant II (Fig. 7): vertical, bottom, horizontal and diagonal cables;

upper and bottom struts. In this case, we express the force densities of the above-mentioned elements normalized respect to those of the bottom struts.

Vertical and bottom cables have analogous behavior, although with different values of force densities; in particular, the minimum degree of geometrical complexity, that is V_{22} topology, corresponds to a minimum value of the force densities, as well as of the internal forces (Figs. 13-16). Notice that such force densities, as well as such internal forces, decrease as the parameter *a* increases. As *a* tends to 1, force densities in these cables tend to the same value.

Moreover, we observe that for the force densities of the horizontal cables the minimum values are obtained for V_{22} topology; moreover, the internal forces vary similarly to those of the horizontal cables of Variant I (Figs. 17, 18), according to the results obtained in [20].

In the same way, internal forces in the diagonal cables exhibit an analogous behavior of that of Variant I. Unlike the Variant I, force densities in the upper struts vary as the parameter *a* goes from 0.1 to 1; in particular, upper struts of class 6 tensegrity, i.e., V_{66} topology, has internal forces greater than corresponding internal forces of class 2 tensegrity, i.e. V_{22} topology (Figs. 19, 20).

Finally, real coefficients α_i, $i = 1, 2, \ldots, n_A$, of Eq. (10) for V_{44} and V_{66} topologies are listed in Tables 5 and 6, respectively.

Table 5

Real coefficients of (10) for V_{44} topology of Variant II

Real coefficients	
α_1	-1
α_2	$\frac{2+\sqrt{2}-\sqrt{2}a}{2(-2+a)a}$

Table 6

Real coefficients of (10) for V_{66} topology of Variant II

Real coefficients	
α_1	-1
α_2	$\frac{-7-4\sqrt{3}+6a+4\sqrt{3}a-3a^2}{2(-2+a)a(-2-\sqrt{3}+\sqrt{3}a)}$

4.3. Variant III

Properties of symmetry of Variant III allows for identifying the following representative elements: vertical, bottom and diagonal cables; struts (Fig. 7). As for Variant I, force densities of such representative elements are normalized respect to the force densities of the struts, which here present the same value.

The analysis of the feasible self-equilibrium states leads to the following observations: for vertical cables, force densities, as well as internal forces, monotonically decrease as the parameter a increases. Among the four considered topologies of Variant III, more complex is the geometry, greater are force densities and internal forces; consequently, the highest values are obtained for V_{66} topology (Figs. 21, 22).

Moreover, for what concerns the bottom cables we observe that as parameter a goes from 0.1 to 1 both the force densities and the internal forces decrease. Notice that for a equal to 0 such force densities tend to the same value (Figs. 23, 24).

Force densities of diagonal cables increase as the parameter a increases, reaching the value 0.5 for a equal to 1. (Figs. 25, 26). Analogously, internal forces in such cables increase as a increases. For such cables, it results that the force densities, as well as the internal forces, assume greater values as the geometrical complexity increases.

4.4. Variant IV

Representative elements of the symmetry groups recognized for Variant IV are vertical, bottom, horizontal and diagonal cables; struts (Fig. 7). In this case too, all the struts are characterized by the same force density, and consequently force densities in the other elements are normalized respect to the force densities of the struts.

From the results of the analysis of the self-equilibrium problem, we have that the force densities of the horizontal cables are equal to 0, and then the corresponding internal forces vanish.

Moreover, we observe that the force densities of the different groups of elements have the same expressions of those of the corresponding elements of Variant III; hence, for Variant IV we have the same properties described above for Variant III.

Finally, we report that the coefficients α_i, $i = 1, 2, \ldots, n_A$, of the linear combinations in (10) for all topologies of Variant IV are equal to 1.

5. Minimal mass analysis: general criteria

In this Section we study the structural efficiency of the examined topologies of the four innovative proposed V-Expander tensegrity cells. To this aim, a possible criterion is that of comparing the minimum structural mass of each cell in the self-equilibrium state. In particular, starting from the axial forces determined in Sect. 4, we assume that both cables and struts are made of structural steel S235 with nominal yield strength $f_y = 235$ N/mm^2,

Young's modulus E = 205000 N/mm^2 and density ρ_s = 7850 kg/m^3, and have a circular cross section. Then, we perform a minimum mass design of the elements according to the design criteria prescribed by Eurocode 3: Design of steel structures - Part 1-1: General rules and rules for buildings [36]. Of course, for cables (in tension) the design constraint is represented by the yielding strength, whereas for struts (in compression) the design constraint comes from the necessity of avoiding buckling. Afterward, the minimum mass of all the elements are summed, in order to have the minimum mass of the cell.

5.1. Struts in compression

Considering the self-equilibrium state, by imposing that the compressive internal force acting on the k-th strut $\tilde{f}_{s,k}$ does not exceed its buckling strength $f_{b,Rd}$ [52], we get the following inequalities:

$$\frac{\tilde{f}_{s,k}}{f_{b,Rd}} \leq 1. \tag{14}$$

For uniform cylindrical steel struts with radius r_s, length l_k, the inertia I_s and the mass m_s can be evaluated as follows, respectively:

$$I_s = \frac{\pi r_s^4}{4}, \tag{15}$$

$$m_s = \rho_s \pi r_s^2 l_{sk}. \tag{16}$$

According to [36], buckling strength for a compression member $f_{b,Rd}$ can be determined as:

$$f_{b,Rd} = \frac{\chi \beta_A A f_y}{\gamma_{M1}}, \tag{17}$$

where β_A is equal to 1 for the adopted class of cross-sectional area A; χ ($\chi \leq 1.0$) represents the reduction factor consistent with the relevant buckling mode, and γ_{M1} is a partial safety factor; in our case it is possible to set γ_{M1} = 1.05.

The value of χ is related to the non-dimensional slenderness $\bar{\lambda}$ of the strut, and can be calculated from the relevant buckling curve equation:

$$\chi = \frac{1}{\phi + \left[\phi^2 - \bar{\lambda}^2\right]^{0.5}}, \tag{18}$$

where

$$\phi = 0.5\left[1 + \alpha\left(\bar{\lambda} - 0.2\right) + \bar{\lambda}^2\right], \tag{19}$$

and the coefficient α is the imperfection factor, corresponding to the appropriate buckling curve. For solid circular cross sectional area, we have to refer to buckling curve *c*, and then $\alpha \cong 0.5$.

The non-dimensional slenderness $\bar{\lambda}$ can be expressed as:

$$\bar{\lambda} = \sqrt{\frac{Af_y}{N_{cr}}}, \tag{20}$$

where N_{cr} is the *Euler elastic critical load*:

$$N_{cr} = \frac{\pi \mathrm{E} I}{l_{sk}^2}. \tag{21}$$

From Eq. (14), by the above equations, we obtain the following expression for the minimal radius $r_{s,\min}$ of the strut, necessary in order to avoid buckling in the self-equilibrium state:

$$r_{s,\min} = \sqrt{\frac{1.05\tilde{\mathrm{f}}_{s,k}}{\pi \chi f_y}}. \tag{22}$$

Substituting Eq. (22) in Eq. (16) we can obtain a lower bound $m_{s,\min}$ for the mass of the strut so that it does not buckle.

5.2. Cables in tension

For what concerns the cables, the following inequality should be verified:

$$\frac{\tilde{\mathrm{f}}_{c,k}}{f_{t,Rd}} \le 1, \tag{23}$$

where $\tilde{\mathrm{f}}_{c,k}$ is the tensile internal force in the *k*-th cable in the feasible self-equilibrium state, and $f_{t,Rd}$ is the tensile strength of the cable.

Let r_c the radius of the circular section of cable; we have:

$$f_{t,Rd} = \frac{\pi r_c^2 f_y}{\gamma_{M1}}, \tag{24}$$

where also in this case it is possible to set $\gamma_{M1} = 1.05$. Then, the minimum radius $r_{c,\min}$ for a cable can be determined by solving the equality in Eq. (23). In particular, we have:

$$r_{c,\min} = \sqrt{\frac{1.05\tilde{\mathrm{f}}_{c,k}}{\pi f_y}}. \tag{25}$$

Inertia I_c and mass m_c of the k-th cable can be obtained by, respectively:

$$I_c = \frac{\pi r_c^4}{4}, \tag{26}$$

$$m_c = \rho_c \pi r_c^2 l_{ck}. \tag{27}$$

Finally, minimum mass for a cable $m_{c,min}$ can be estimated by substituting in Eq. (27) the expression in Eq. (25) for the radius of the cross section.

6. Minimal mass analysis: results and comparison

From the results of the analyses of the feasible self-equilibrium states (Sect. 4) it is possible to evaluate the maximum internal forces in the elements – compression for struts and tension for cables – for each of the examined V-Expander tensegrity cells. Then, according to the criteria in Sect. 5, by determining the minimum mass of the elements, struts and cables, respectively, it is finally possible to obtain the minimal masses of the considered V-Expander tensegrity cell.

In particular, once considered a V-Expander tensegrity cell (of a particular variant and having a particular topology), its minimal total mass can be evaluated by means of the following steps:

1. From the self-equilibrium analysis in Sect. 4, determine the maximum compressive internal force $\tilde{f}_{s,max}$ for the struts and the maximum tensile internal force $\tilde{f}_{c,max}$ for the cables;
2. Calculate minimal radius $r_{s,min}$ of the struts (see Sect. 5.1) and minimal radius $r_{c,min}$ of the cables (see Sect. 5.2) consistent with the maximum internal forces;
3. Determine the minimum mass for the struts $m_{s,min}$ according to Sect. 5.1 and the minimum mass for the cable $m_{c,min}$ according to Sect. 5.2;
4. Evaluate the minimal total mass of the cell M_{tot} by Eq. (28).

$$M_{tot} = M_{c,min} + M_{s,min} = \sum_{i=1}^{c} m_{c,min} + \sum_{i=1}^{s} m_{s,min} = \sum_{i=1}^{c} \rho_c \pi r_{c,min}^2 l_{sk} + \sum_{i=1}^{s} \rho_s \pi r_{s,min}^2 l_{ck}, \tag{28}$$

where $r_{s,min}$ and $r_{c,min}$ can be determined by using Eq. (22) and Eq. (25), respectively. Notice that in Eq. (28) the total mass M_{tot} of the V-Expander tensegrity cell is a function of the parameter a, that varies in the range defined in Sect. 3.

Thereby, it is possible to compare the total masses for each of the examined topology of the four variants of the V-Expander tensegrity cells analyzed, i.e., for V_{22}, V_{33}, V_{44}, and V_{66}. The aim of this analysis is the evaluation of

the efficiency of the innovative V-Expander tensegrity cells proposed in [20] in terms of the possible reduction of the total mass of the structure as the degree of geometric complexity increases.

First, let us consider the topology V_{22}, and let us compare the efficiency of the four Variants I, II, III and IV in terms of minimal total mass M_{tot}. The results of this comparison are shown in Fig. 27. We observe that, as *a* that varies from 0.1 to 1, Variant I is characterized by the lowest minimal total mass with respects of the other examined Variants. On the contrary, the highest minimal total mass is that of Variant II for each *a* in the considered range. The minimal total mass of Variant III is lesser than that of Variant IV; both are slightly higher than the minimal total mass of Variant I; for example, for $a = 0.6$, the minimal total mass of Variant IV differs from the minimal total mass of Variant I of about 6%. Moreover, as *a* approaches 1, the minimal total mass of Variant III tends to be equal to that of Variant I.

We consider then the topology V_{33}, and discuss again the efficiency of the four Variants I, II, III and IV in terms of minimal total mass M_{tot}. The results of this comparison are shown in Fig. 28. In this case, for *a* ranging from 0.1 to about 0.7, Variant I is characterized by the lowest minimal total mass; on the other hand, for $a > 0.7$ the lowest minimal total mass is that of Variant III. Notice that Variant III has a more complex geometry with respect to Variant I: thus, for the examined topology V_{33} it is possible to affirm that (at least for $a > 0.7$) a more complex geometry corresponds to a higher efficiency. For each *a* in the considered range, the highest minimal total mass is that of Variant II, as in the previous case. Moreover, we observe that the differences between the minimal total masses of Variants I, III and IV are very low: for example, for $a = 0.6$, the minimal total mass of Variant IV (the highest among the three considered) differs from the minimal total mass of Variant I (the lowest among the three considered) of about 7%.

We now pass to the topology V_{44}, and compare the efficiency of the four Variants I, II, III and IV in terms of minimal total mass M_{tot}. The results of this comparison are shown in Fig. 29. We have substantially the same results discussed for the topology V_{33}, except for the fact that the lowest minimal total mass is that of Variant I for *a* ranging from 0.1 to about 0.8, and of Variant III for $a > 0.8$.

Finally, we consider the topology V_{66}, discussing the efficiency of the four Variants I, II, III and IV in terms of minimal total mass M_{tot}. The results of this comparison are shown in Fig. 30. In this case, the results are rather similar to that obtained for the topology V_{22}: Variant I and Variant II are characterized by the lowest and the highest minimal total mass, respectively, as *a* that varies from 0.1 to 1. The minimal total mass of Variant III is lesser than that of Variant IV; both the minimal total masses tends to that of Variant I as *a* approaches 1. The remarkable difference between the topology V_{66} and the topology V_{22} is that for small values of *a* the minimal total masses of Variants III and Variant IV are substantially higher than that of Variant I.

The above analyses show that for all the considered topologies Variant II is the less efficient, since it is characterized by a far greater minimal total mass. Indeed, from the analyses of feasible self-stress states for

Variant II it emerges that, for reasons related to symmetry properties, the compressive forces in the upper struts are greater than the compressive forces in the bottom struts. Exclusively for a which tends to 1 both bottom and upper struts tend to have the same value of the compressive internal forces. On the contrary, either for Variant I, and for Variant III and for Variant IV all the struts are characterized by the same compressive internal forces: this uniformity justifies the fact that the highest value of the maximum compressive forces for Variants I, III and IV are lower than those for Variant II.

Moreover, it is worth to note that, for all topologies analyzed, minimum masses of tensegrity cells decrease as the length of the vertical cable increases, that is, for a that goes from 0.1 to 1, due to the decreasing of the total masses of the cables.

Finally, we can state that for a that ranges from 0.1 to 0.7 (or to 0.8 for topologies V_{33} and V_{44}) the minimum total mass of Variant I is the lowest minimum total mass among the other examined variants; on the other hand, for $a > 0.7$ (or to 0.8 for topologies V_{33} and V_{44}) the lowest minimum total mass is that of Variant III. Anyway, the minimum total masses of Variant I and III only slightly differ: for example, in the right neighborhood of 0.1 minimum masses of Variant III differs from the minimum masses of Variant I of about 13.9%, 16.7%, 17.7% and 34.6% for V_{22}, V_{33}, V_{44} and V_{66} topologies, respectively.

7. Conclusions

We propose a study of the mechanical behavior of the innovative V-Expander tensegrity cells proposed in [20] aimed at analyzing the feasible self-stress states of these tensegrity elementary cells in different topologies, that are obtained by increasing the number of struts forming the elements in compression the cell. In particular, we perform the analyses of the self-equilibrium states of four out of five innovative cells, i.e., Variant I, II, III and IV, in the cases in which the components in compression are made of 2 (topology V_{22}), 3 (topology V_{33}), 4 (topology V_{44}) and 6 struts (topology V_{66}), respectively.

The self-equilibrium analyses are parameterized by using only three parameters (h, r and a), governing the morphology of the cells. By fixing two out of these three parameters (h, and r), it is possible to describe how the force densities and the internal forces in the elements in the feasible self-equilibrium states vary as the parameter a changes in a representative range of values.

Results presented in Section 4 point out that it can be identified a peculiar mechanical behavior of the representative elements of the V-Expander tensegrity cells according to the properties of the symmetry of each variant.

According to the obtained results, some observations about the morphological aspects of the assembly of the examined V-expander tensegrity cells can be point out. Variant I, II and IV lend themselves more easily to realization of tensegrity grids due to the presence of horizontal cables [35]. Tensegrity chains can be easily obtained by assembling Variant III tensegrity cells in the direction of the vertical cable. Tensegrity chains obtained by means of juxtaposition of Variant I, II and IV, respectively, permit smaller variation of the geometry due to horizontal cables overlapping. Furthermore, further studies on mixed assemblies of such variants, in order to build planar or curved grids, roofs, columns or chains as well as arches, should be carry out.

Moreover, by solving the mass minimization problem in the feasible self-equilibrium states according to the member design criteria in Eurocode 3 [36], we discuss how the minimal total masses M_{tot} of the tensegrity cells vary as the parameter a changes. We evaluate the efficiency of these innovative V-Expander tensegrity cells for each of the considered topologies in terms of minimal total masses. We observe that to a higher degree of complexity does not always correspond an increase of the minimal total mass of the structure; indeed, Variant III and Variant IV have about the same minimal total mass of Variant I, especially for values of the parameter a which tend to 1.

This work will constitute the basis for facing the mass minimization problem for complex tensegrity structures composed of assemblies of the considered innovative V-Expander tensegrity cells. Moreover, the mass minimization problem will be developed by also considering the effects of external loads.

References

[1] Ferkiss V, Fuller RB, Applewhite EJ. Synergetics: Explorations in the Geometry of Thinking. Technol Cult 1976;17:104. doi:10.2307/3103256.

[2] Jáuregui VG. Controversial Origins of Tensegrity. Proc Int Assoc Shell Spat Struct 2009:1642–52.

[3] Amendola A, Hernández-Nava E, Goodall R, Todd I, Skelton RE, Fraternali F. On the additive manufacturing, post-tensioning and testing of bi-material tensegrity structures. Compos Struct 2015;131:66–71. doi:10.1016/j.compstruct.2015.04.038.

[4] Rimoli JJ, Pal RK. Mechanical response of 3-dimensional tensegrity lattices. Compos Part B Eng 2017;115:30–42. doi:10.1016/j.compositesb.2016.10.046.

[5] Magliozzi L, Micheletti A, Pizzigoni A, Ruscica G. On the design of origami structures with a continuum of equilibrium shapes. Compos Part B Eng 2017;115:144–50. doi:10.1016/j.compositesb.2016.10.023.

[6] De Oliveira MC, Skelton RE. Tensegrity systems. 2009. doi:10.1007/978-0-387-74242-7.

[7] Lewis WJ (Wanda J. Tension structures : form and behaviour. Thomas Telford; 2003.

[8] Lee S, Gan BS, Lee J. A fully automatic group selection for form-finding process of truncated tetrahedral tensegrity structures via a double-loop genetic algorithm. Compos Part B Eng 2016;106:308–15. doi:10.1016/j.compositesb.2016.09.018.

[9] Yuan XF, Ma S, Jiang SH. Form-finding of tensegrity structures based on the Levenberg–Marquardt method. Comput Struct 2017;192:171–80. doi:10.1016/j.compstruc.2017.07.005.

[10] Koohestani K, Guest SD. A new approach to the analytical and numerical form-finding of tensegrity structures. Int J Solids Struct 2013;50:2995–3007. doi:10.1016/j.ijsolstr.2013.05.014.

[11] Klinka K, Arcaro V, Gasparini D. Form finding of tensegrity structures using finite elements and mathematical programming. J Mech Mater Struct 2012;7:899–907. doi:10.2140/jomms.2012.7.899.

[12] Zhang L-Y, Zhu S-X, Li S-X, Xu G-K. Analytical form-finding of tensegrities using determinant of force-density matrix. Compos Struct 2018;189:87–98. doi:10.1016/J.COMPSTRUCT.2018.01.054.

[13] Koohestani K. On the analytical form-finding of tensegrities. Compos Struct 2017;166:114–9. doi:10.1016/j.compstruct.2017.01.059.

[14] Veenendaal D, Block P. An overview and comparison of structural form finding methods for general networks. Int J Solids Struct 2012;49:3741–53. doi:10.1016/j.ijsolstr.2012.08.008.

[15] Tibert AG, Pellegrino S. Review of Form-Finding Methods for Tensegrity Structures. Int J Sp Struct

2011;26:241–55. doi:10.1260/0266-3511.26.3.241.

[16] Juan SH, Mirats Tur JM. Tensegrity frameworks: Static analysis review. Mech Mach Theory 2008;43:859–81. doi:10.1016/j.mechmachtheory.2007.06.010.

[17] Harichandran A, Yamini Sreevalli I. Form-Finding of Tensegrity Structures based on Force Density Method. Indian J Sci Technol 2016;9. doi:10.17485/ijst/2016/v9i24/93145.

[18] Linkwitz K. Formfinding by the "Direct Approach" and Pertinent Strategies for the Conceptual Design of Prestressed and Hanging Structures. Int J Sp Struct 1999;14:73–87. doi:10.1260/0266351991494713.

[19] Schek HJ. The force density method for form finding and computation of general networks. Comput Methods Appl Mech Eng 1974;3:115–34. doi:10.1016/0045-7825(74)90045-0.

[20] Fraddosio A, Marzano S, Pavone G, Piccioni MD. Morphology and self-stress design of V-Expander tensegrity cells. Compos Part B Eng 2017;115:102–16. doi:10.1016/j.compositesb.2016.10.028.

[21] Maurin B, Motro R, Raducanu V, Pauli N. Soft "tensegrity like" panel: Conceptual design and Form - Finding. J Int Assoc Shell Spat Struct 2008;49:77–87.

[22] Motro R. Tensegrity : from Art to Structural Engineering 1958.

[23] Motro R. Tensegrity: Structural Systems for the Future. 2003. doi:10.1016/B978-1-903996-37-9.X5028-8.

[24] Sarma KC, Adeli H. Cost optimization of steel structures. Eng Optim 2000. doi:10.1080/03052150008941321.

[25] Nagase K, Skelton RE. Minimal mass tensegrity structures. J Int Assoc Shell Spat Struct 2014;55:37–48. doi:10.1117/12.2044869.

[26] Skelton RE, Fraternali F, Carpentieri G, Micheletti A. Minimum mass design of tensegrity bridges with parametric architecture and multiscale complexity. Mech Res Commun 2014;58:124–32. doi:10.1016/j.mechrescom.2013.10.017.

[27] Fraternali F, Carpentieri G, Modano M, Fabbrocino F, Skelton RE. A tensegrity approach to the optimal reinforcement of masonry domes and vaults through fiber-reinforced composite materials. Compos Struct 2015;134:247–54. doi:10.1016/j.compstruct.2015.08.087.

[28] Skelton RE, Montuori R, Pecoraro V. Globally stable minimal mass compressive tensegrity structures. Compos Struct 2016;141:346–54. doi:10.1016/j.compstruct.2016.01.105.

[29] de Oliveira MC, Skelton RE, Chan W. Minimum Mass Design of Tensegrity Towers and Plates. Proc

45th IEEE Conf Decis Control 2006:2314–9. doi:10.1109/CDC.2006.377427.

[30] Gómez-Jáuregui V, Arias R, Otero C, Manchado C. Novel Technique for Obtaining Double-Layer Tensegrity Grids. Int J Sp Struct 2012. doi:10.1260/0266-3511.27.2-3.155.

[31] Zhang LY, Li SX, Zhu SX, Zhang BY, Xu GK. Automatically assembled large-scale tensegrities by truncated regular polyhedral and prismatic elementary cells. Compos Struct 2018;184:30–40. doi:10.1016/j.compstruct.2017.09.074.

[32] Angellier N, Dubé JF, Quirant J, Crosnier B. Behavior of a Double Layer Tensegrity Grid under Static Loading: Identification of Self-Stress Level. J Struct Eng 2012;139:120903010853001. doi:10.1061/(ASCE)ST.1943-541X.0000710.

[33] Smaili A, Motro R. Foldable / unfoldable curved tensegrity systems by finite mechanism activation. J. Int. Assoc. Shell Spat. Struct., vol. 48, 2007, p. 153–60.

[34] Gomez-Jauregui V, Otero C, Arias R, Manchado C. Innovative Families of Double-Layer Tensegrity Grids: Quastruts and Sixstruts. J Struct Eng 2012:120917004002007. doi:10.1061/(ASCE)ST.1943-541X.0000739.

[35] Fraddosio A, Pavone G, Piccioni MD. New V-Expander tensegrity grids: design of self-stress states n.d. doi:10.1016/j.compositesb.2016.10.028.

[36] EN 1993-1-1. Eurocode 3: Design of steel structures - Part 1-1: General rules and rules for buildings. Eurocode 3 2005;1:91 pp. doi:[Authority: The European Union Per Regulation 305/2011, Directive 98/34/EC, Directive 2004/18/EC].

[37] Zhang L-Y, Li Y, Cao Y-P, Feng X-Q, Gao H. A Numerical Method for Simulating Nonlinear Mechanical Responses of Tensegrity Structures Under Large Deformations. J Appl Mech 2013;80:061018. doi:10.1115/1.4023977.

[38] Guest SD. The stiffness of tensegrity structures. IMA J Appl Math (Institute Math Its Appl 2011;76:57–66. doi:10.1093/imamat/hxq065.

[39] Zhang JY, Ohsaki M. Adaptive force density method for form-finding problem of tensegrity structures. Int J Solids Struct 2006;43:5658–73. doi:10.1016/j.ijsolstr.2005.10.011.

[40] Calladine CR. Buckminster Fuller's "Tensegrity" structures and Clerk Maxwell's rules for the construction of stiff frames. Int J Solids Struct 1978;14:161–72. doi:10.1016/0020-7683(78)90052-5.

[41] Pellegrino S, Calladine CR. Matrix analysis of statically and kinematically indeterminate frameworks. Int J Solids Struct 1986;22:409–28. doi:10.1016/0020-7683(86)90014-4.

[42] Tran HC, Lee J. Form-finding of tensegrity structures with multiple states of self-stress. Acta Mech 2011;222:131–47. doi:10.1007/s00707-011-0524-9.

[43] Koohestani K. Form-finding of tensegrity structures via genetic algorithm. Int J Solids Struct 2012;49:739–47. doi:10.1016/j.ijsolstr.2011.11.015.

[44] Chen Y, Feng J, Ma R, Zhang Y. Efficient symmetry method for calculating integral prestress modes of statically indeterminate cable-strut structures. J Struct Eng 2015;141:04014240. doi:10.1061/(ASCE)ST.1943-541X.0001228.

[45] Yuan XF, Dong SL. Integral feasible prestress of cable domes. Comput Struct 2003;81:2111–9. doi:10.1016/S0045-7949(03)00254-2.

[46] Yuan X, Chen L, Dong S. Prestress design of cable domes with new forms. Int J Solids Struct 2007;44:2773–82. doi:10.1016/j.ijsolstr.2006.08.026.

[47] Tran HC, Lee J. Advanced form-finding of tensegrity structures. Comput Struct 2010;88:237–46. doi:10.1016/j.compstruc.2009.10.006.

[48] Ehara S, Kanno Y. Topology design of tensegrity structures via mixed integer programming. Int J Solids Struct 2010;47:571–9. doi:10.1016/j.ijsolstr.2009.10.020.

[49] Lee S, Lee J. A novel method for topology design of tensegrity structures. Compos Struct 2016;152:11–9. doi:10.1016/j.compstruct.2016.05.009.

[50] Motro R. Structural morphology of tensegrity systems. Meccanica 2011;46:27–40. doi:10.1007/s11012-010-9379-8.

[51] Quirant J, Kazi-Aoual MN, Motro R. Designing tensegrity systems: The case of a double layer grid. Eng Struct 2003;25:1121–30. doi:10.1016/S0141-0296(03)00021-X.

[52] Bazant ZP, Cedolin L, Hutchinson JW. Stability of Structures: Elastic, Inelastic, Fracture, and Damage Theories. J Appl Mech 1993;60:567. doi:10.1115/1.2900839.

Figures

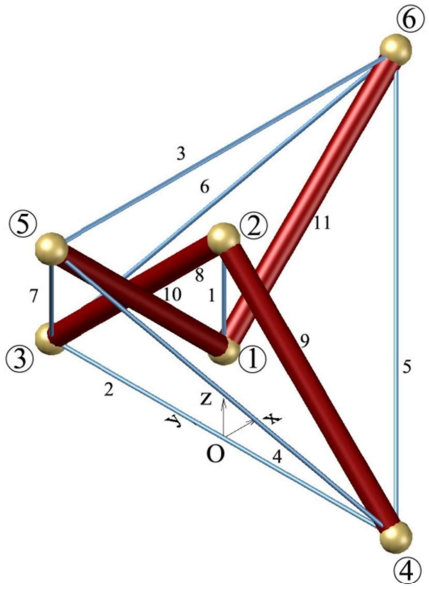

Fig.1 Variant I

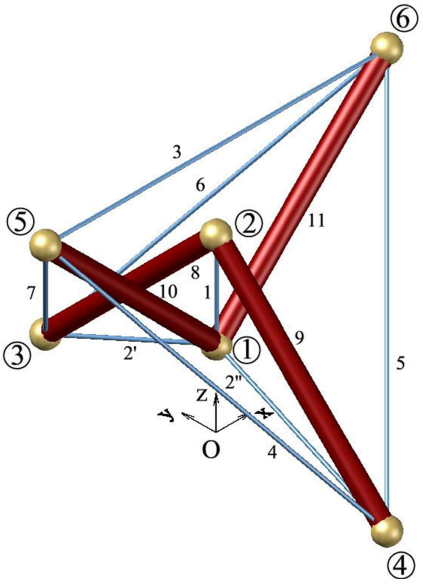

Fig.2 Variant II

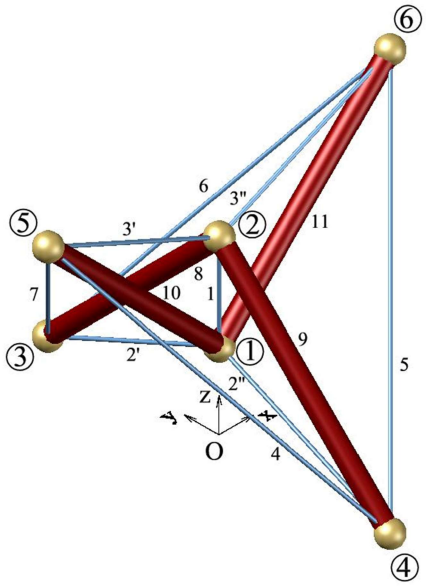

Fig.3 Variant III

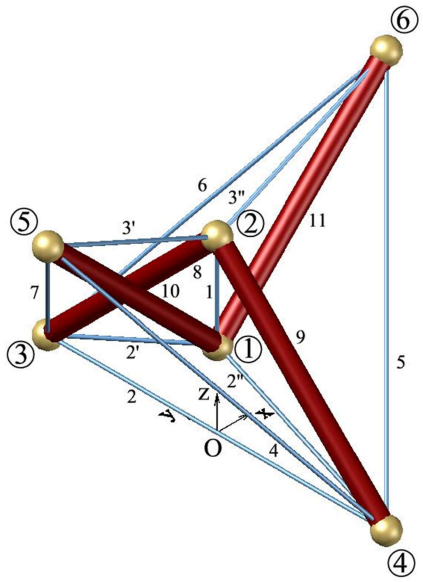

Fig.4 Variant IV

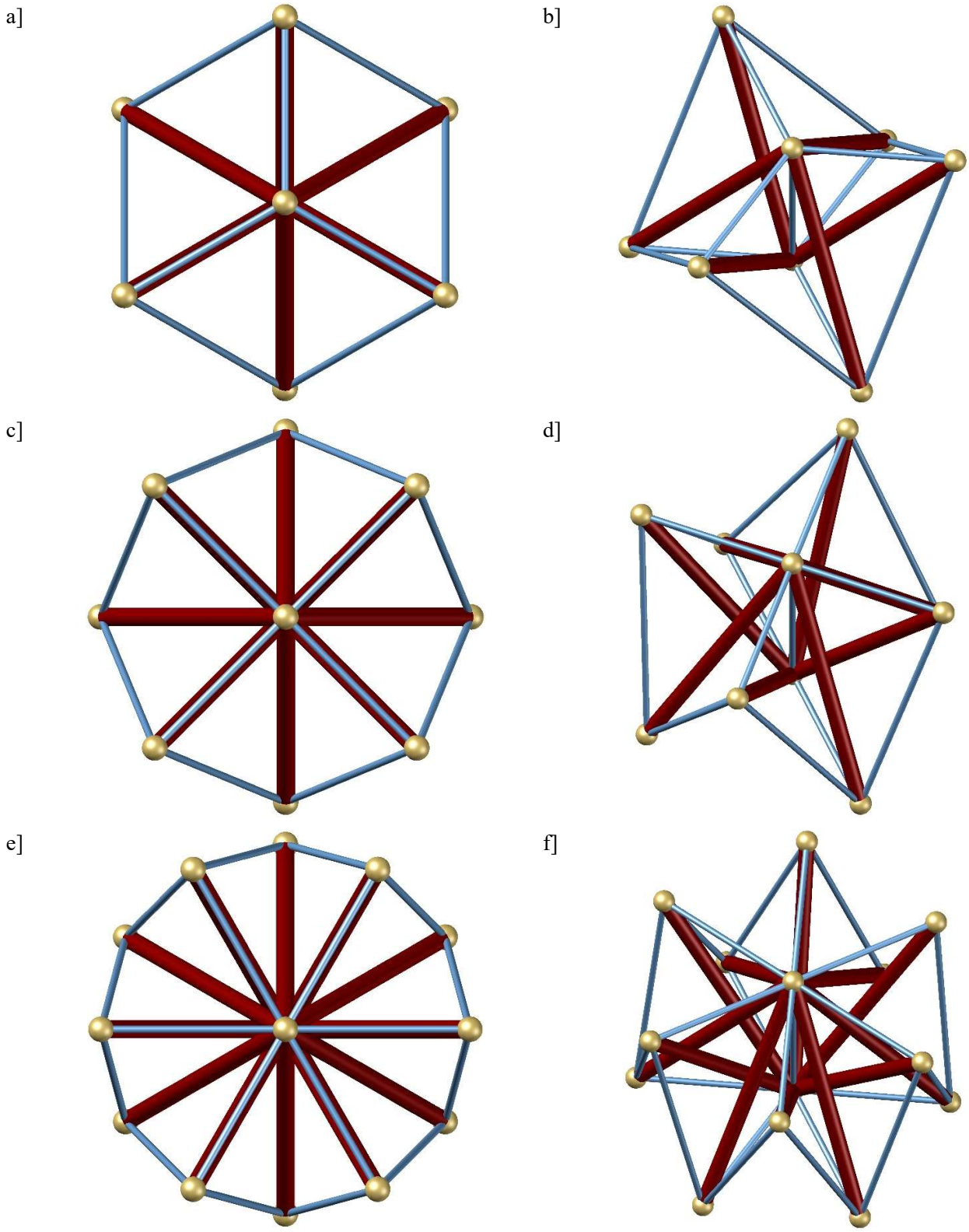

Fig.5 Different topologies of Variant III ($d = h$): a] V_{33}-Expander top view, b] V_{33}-Expander axonometric view, c] V_{44}-Expander top view, d] V_{44}-Expander axonometric view, e] V_{66}-Expander top view, f] V_{66}-Expander axonometric view. (axonometric view of V_{22}-Expander of Variant III is shown in Fig. 3)

a] b]

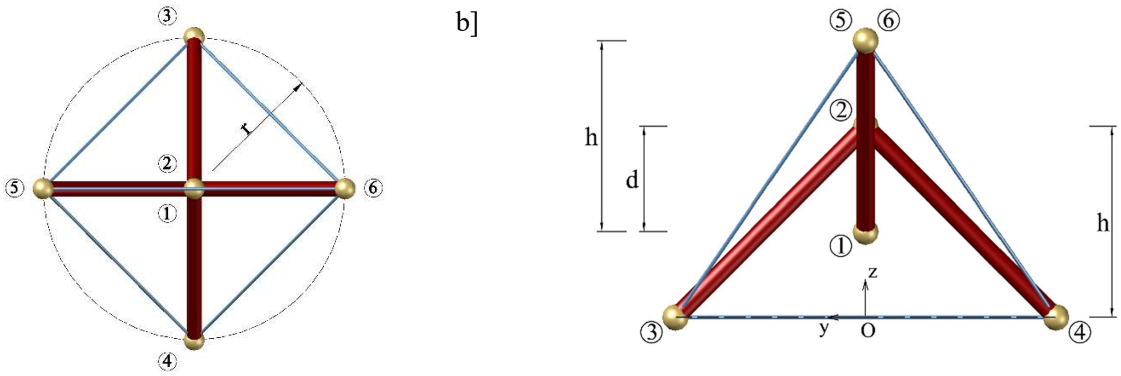

Fig.6 Parametric description of geometry of the V_{22}-Expander cell: a] top view (Variant I), b] lateral view (Variant I).

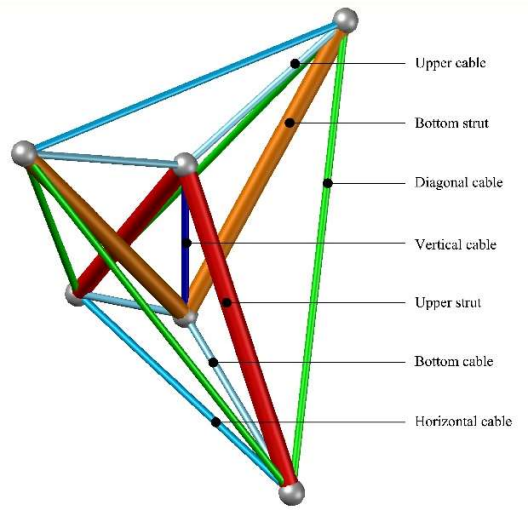

Fig.7 Representative elements of the V_{22}-Expander cells.

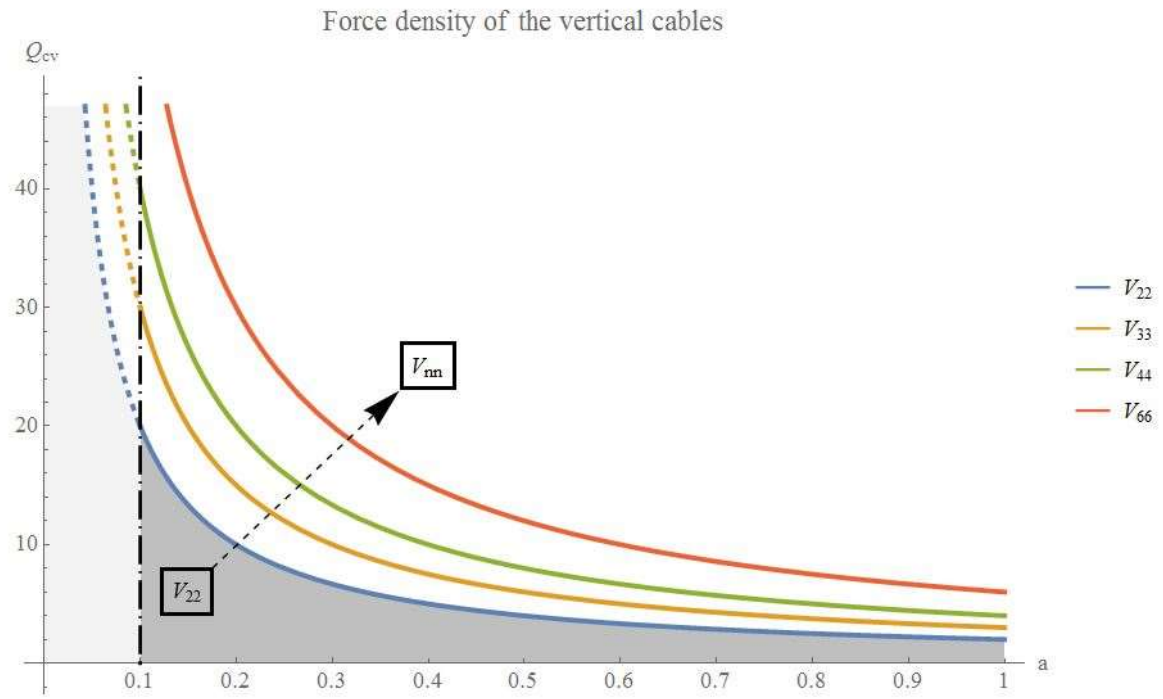

Fig.8 Variation of force densities of the vertical cables of Variant I.

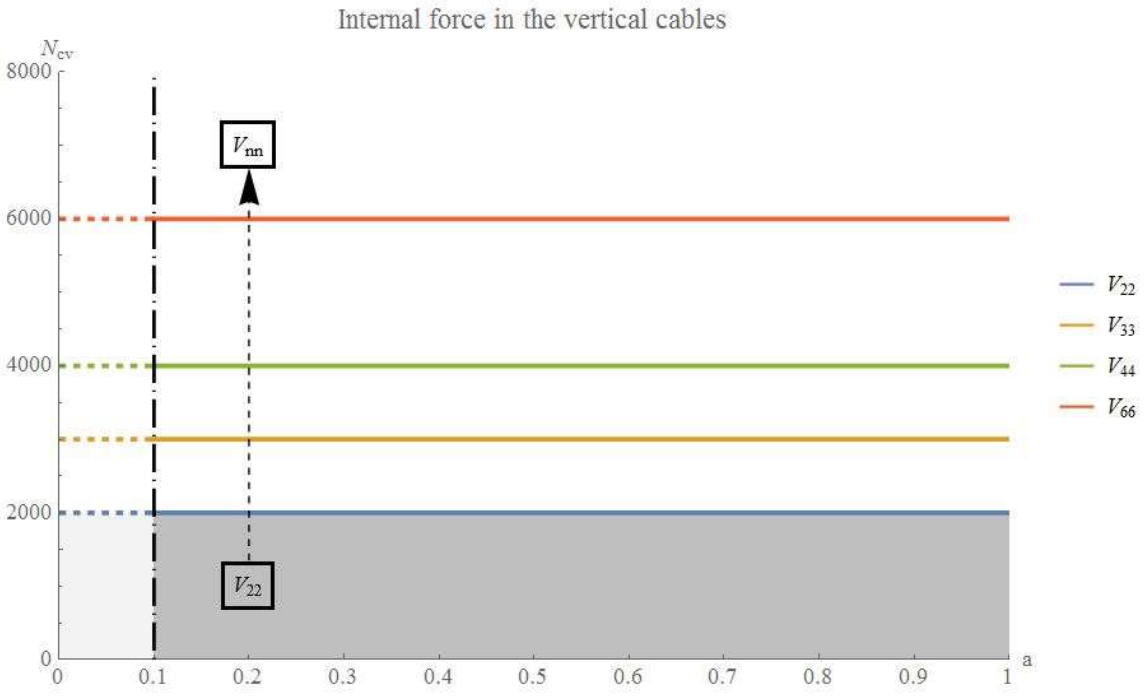

Fig.9 Variation of internal forces in the vertical cables of Variant I.

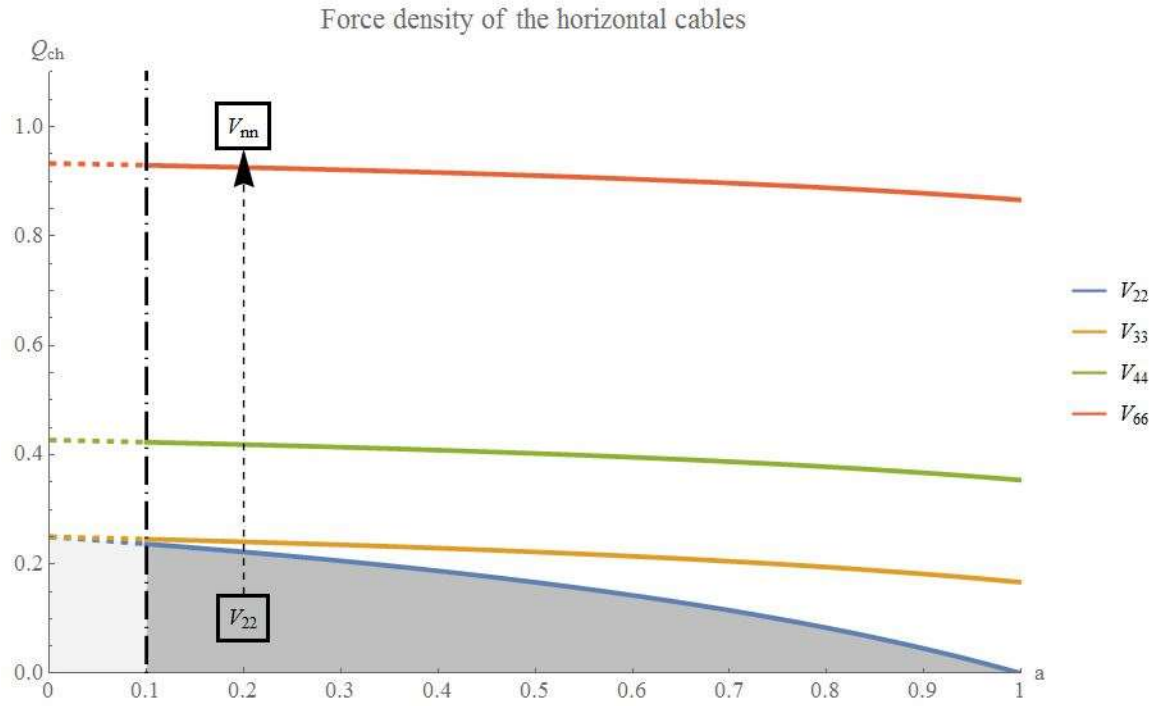

Fig.10 Variation of force densities of the horizontal cables of Variant I.

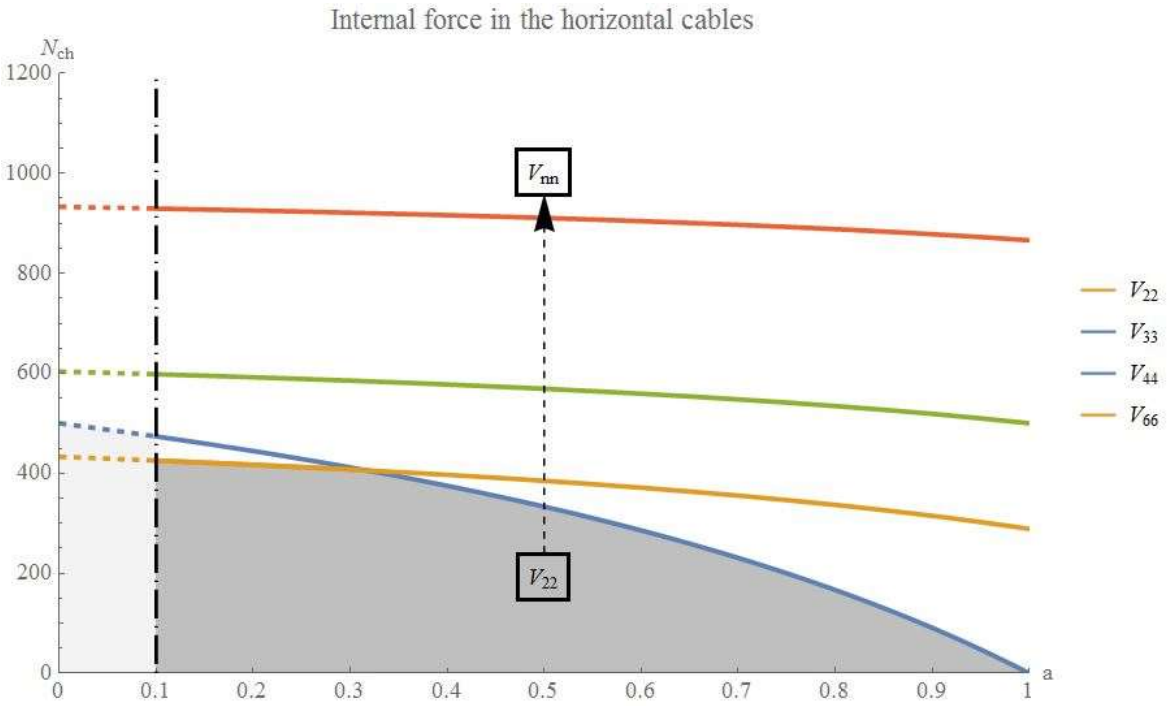

Fig.11 Variation of internal forces in the horizontal cables of Variant I. For $0.1 < a < 0.317$ lower bound of the internal forces is V_{22} topology.

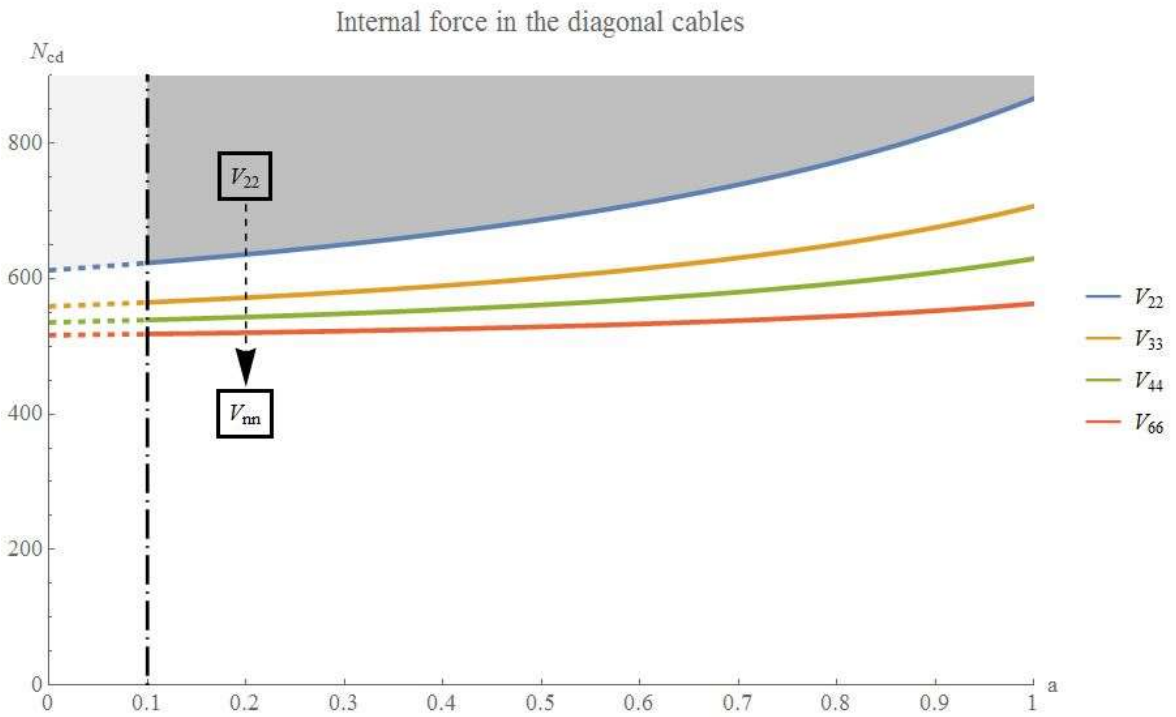

Fig.12 Variation of internal forces in the diagonal cables of Variant I.

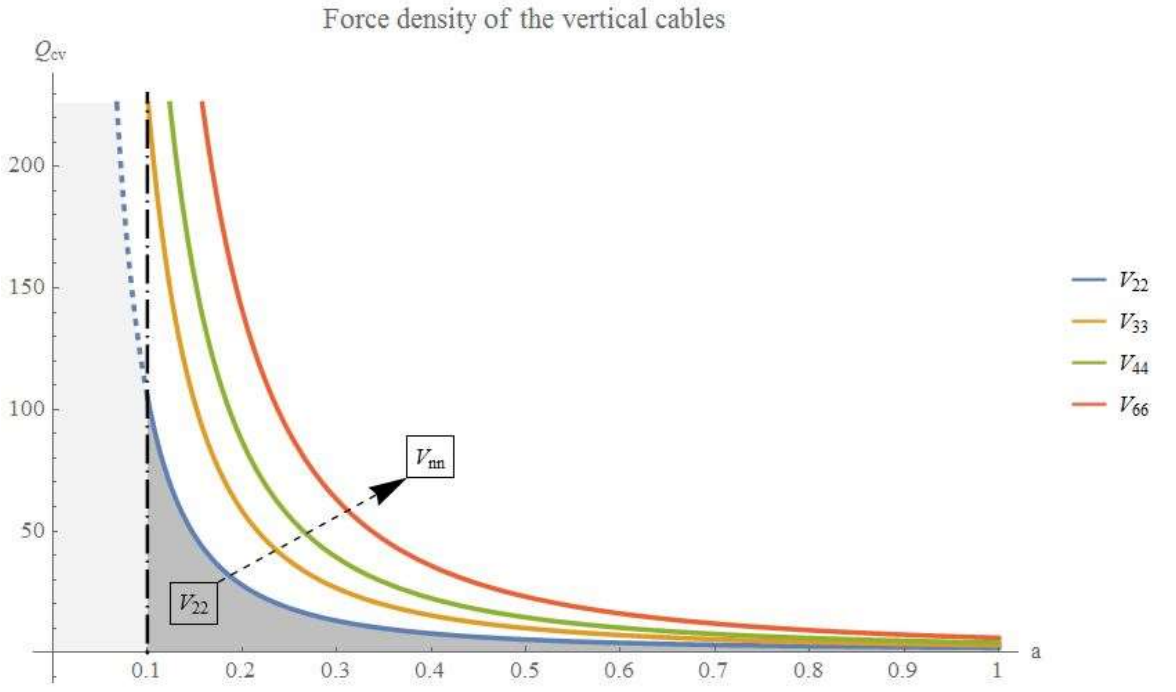

Fig.13 Variation of force densities of the vertical cables of Variant II.

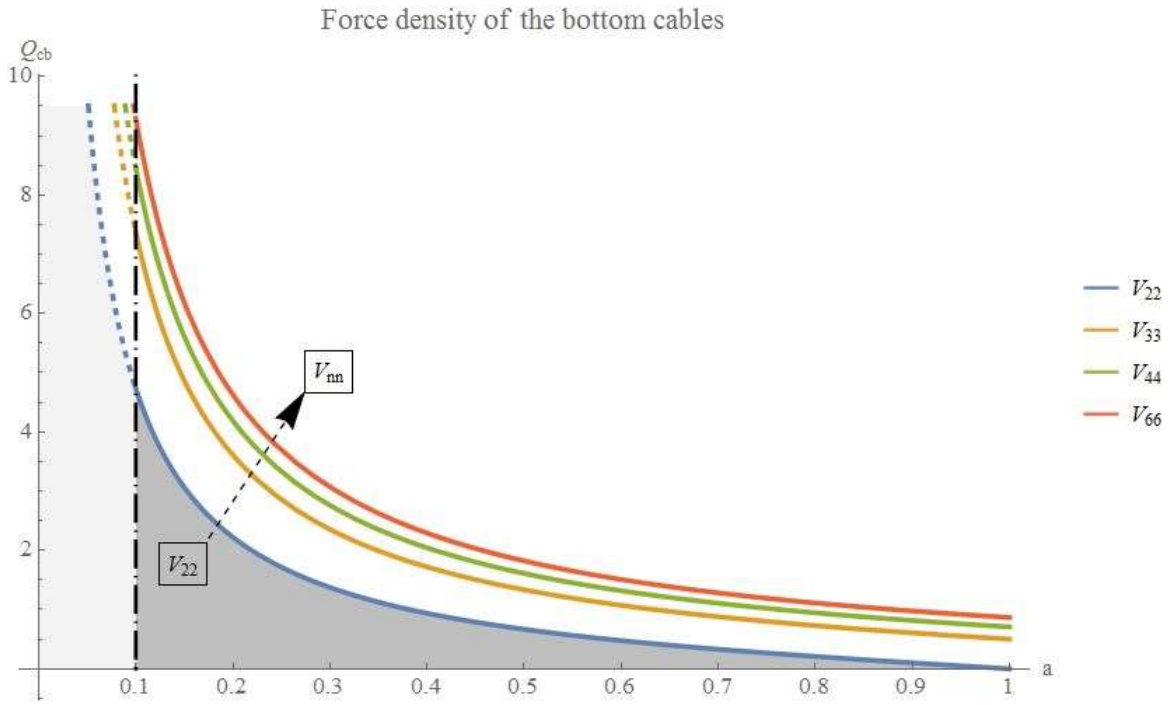

Fig.14 Variation of force densities of the bottom cables of Variant II.

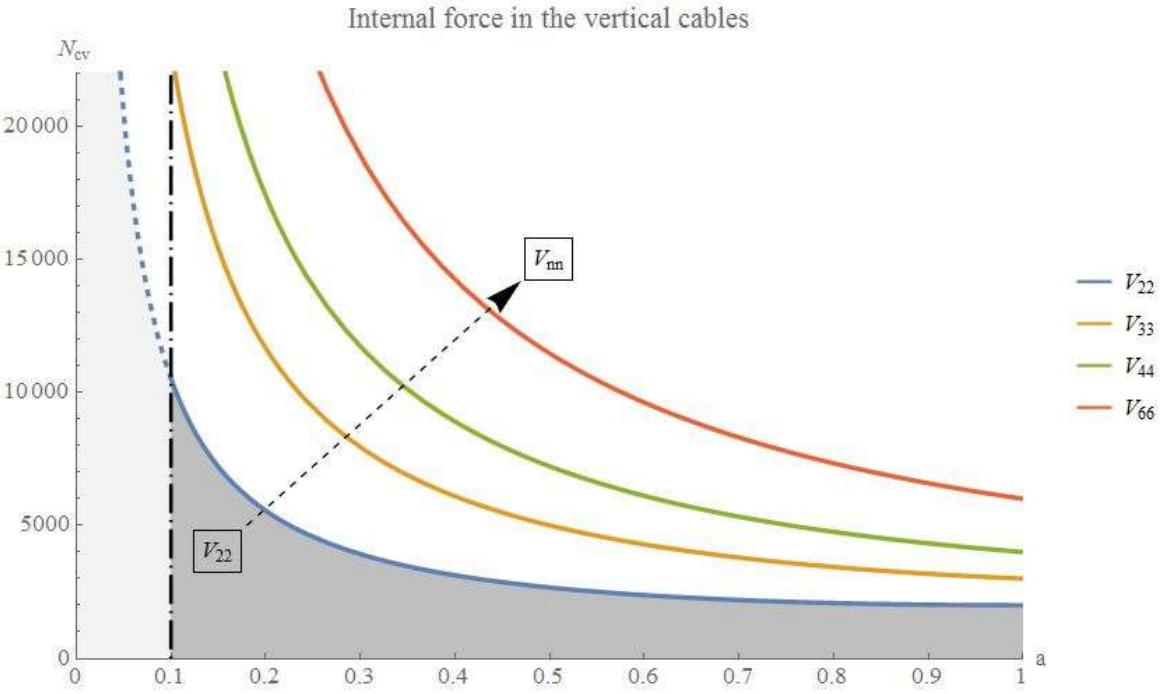

Fig.15 Variation of internal forces in the vertical cables of Variant II.

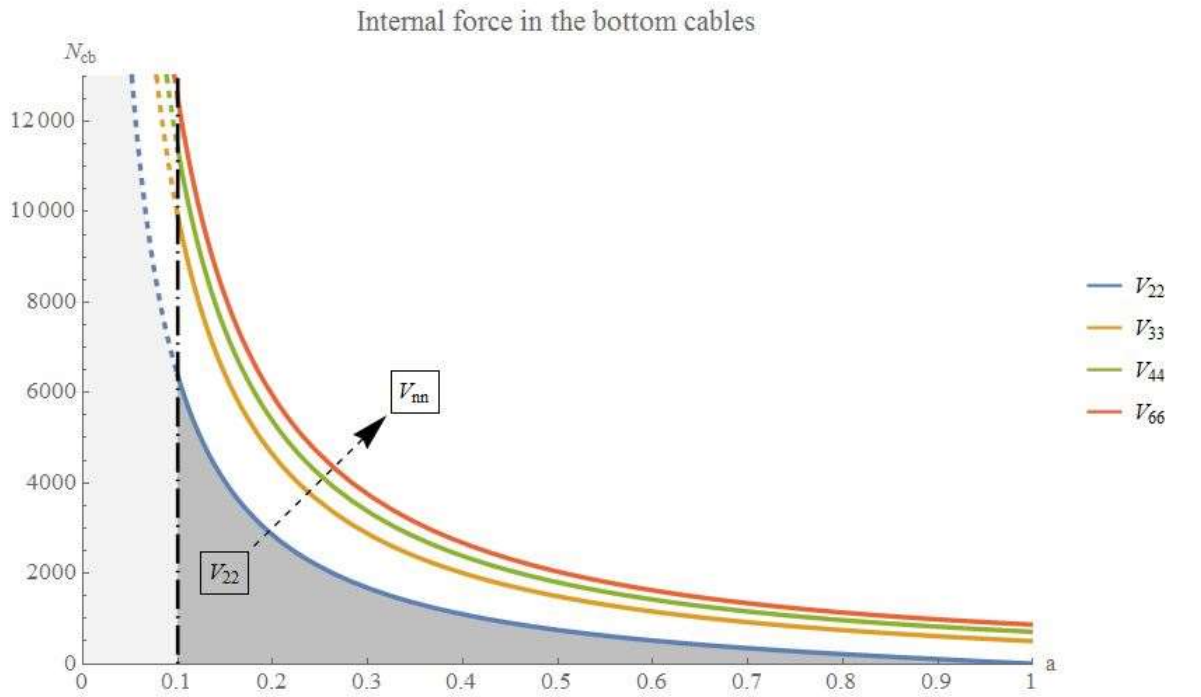

Fig.16 Variation of internal forces in the bottom cables of Variant II.

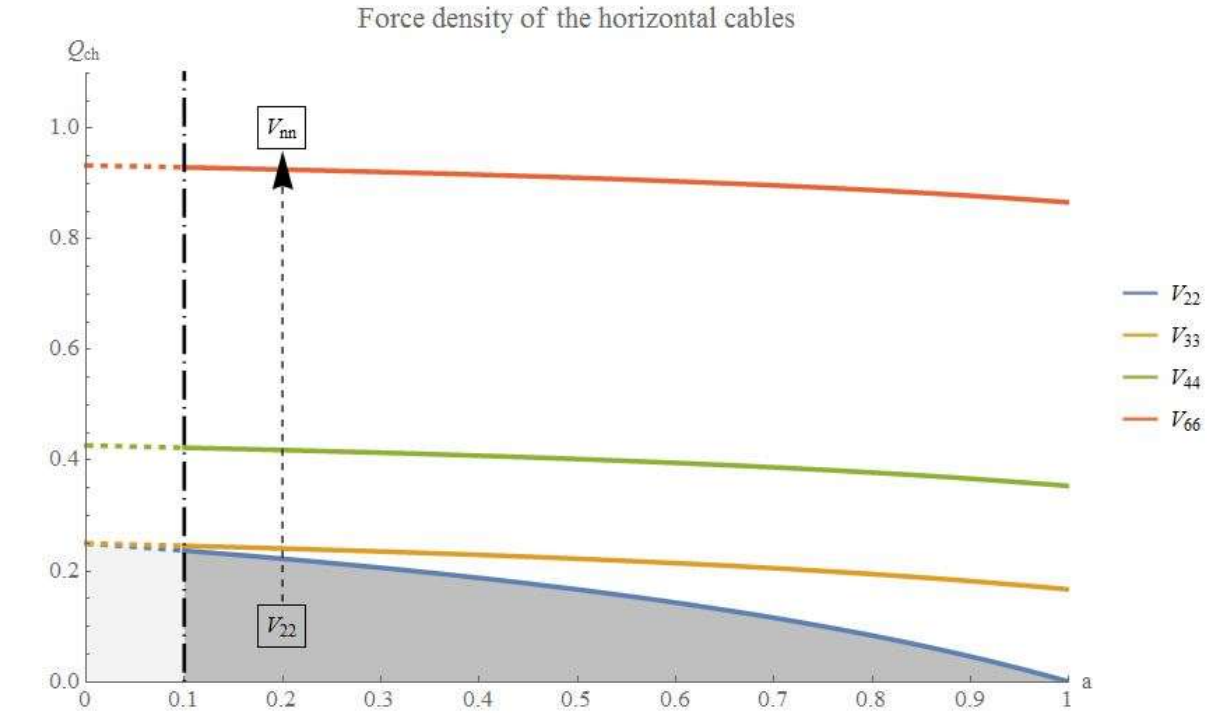

Fig.17 Variation of force densities of the horizontal cables of Variant II.

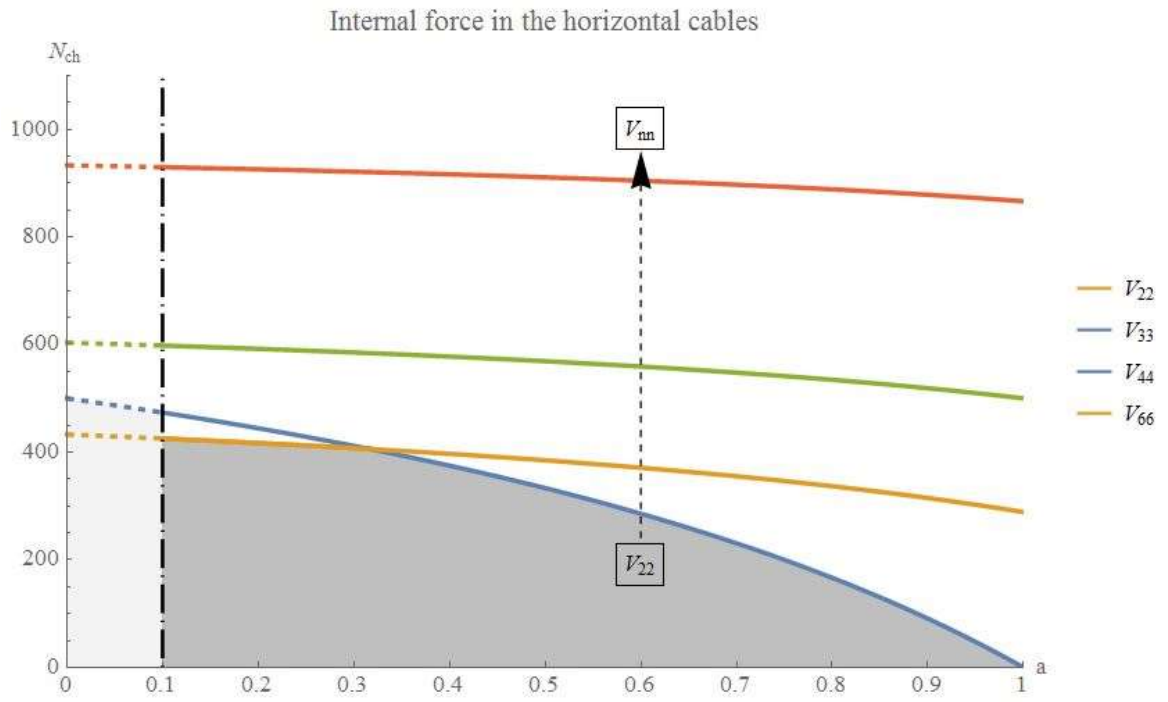

Fig.18 Variation of internal forces in the horizontal cables of Variant II. For $0.1 < a < 0.317$ lower bound of the internal forces is V_{22} topology.

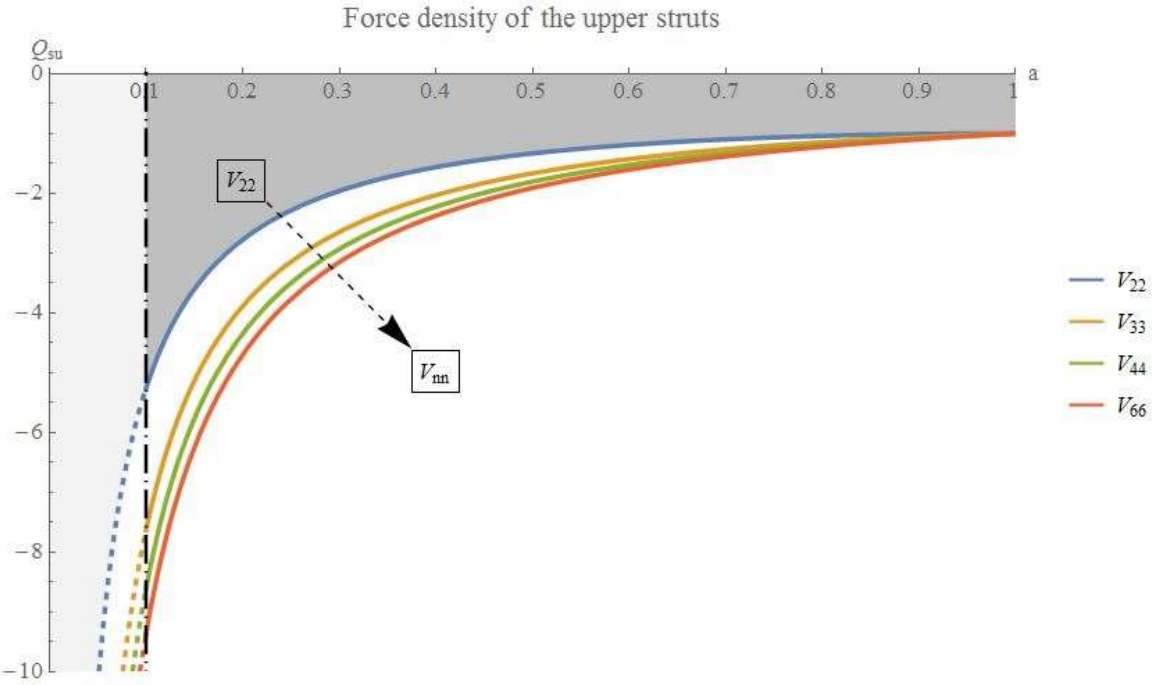

Fig.19 Variation of force densities of the upper struts of Variant II.

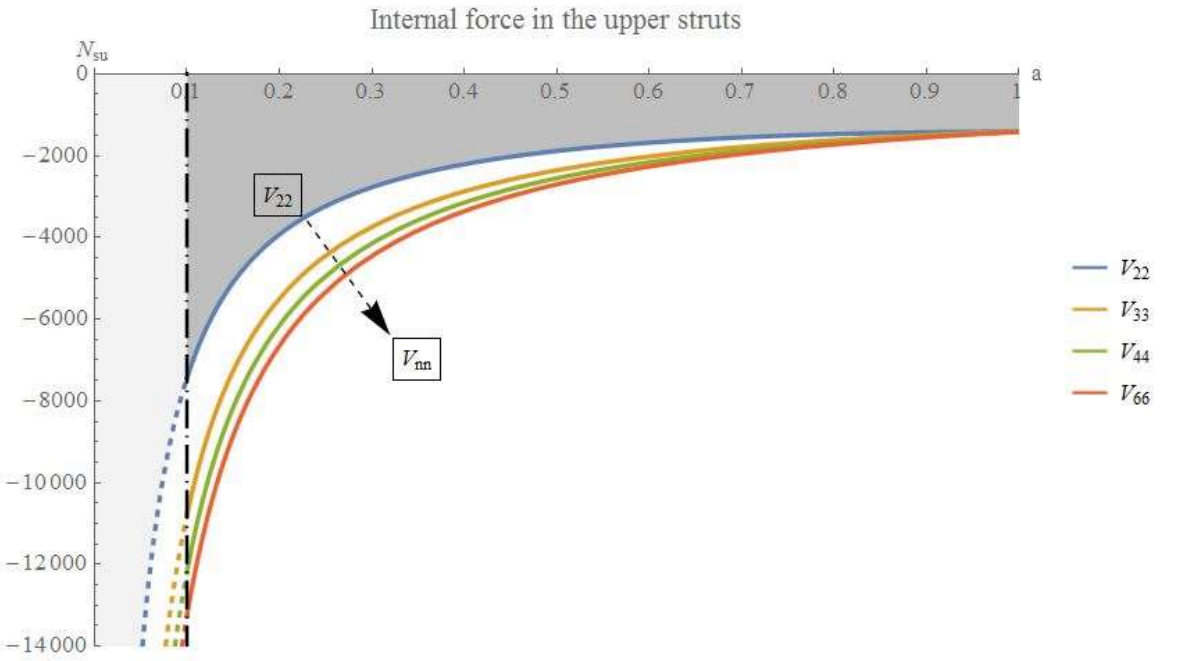

Fig.20 Variation of internal forces in the upper struts of Variant II.

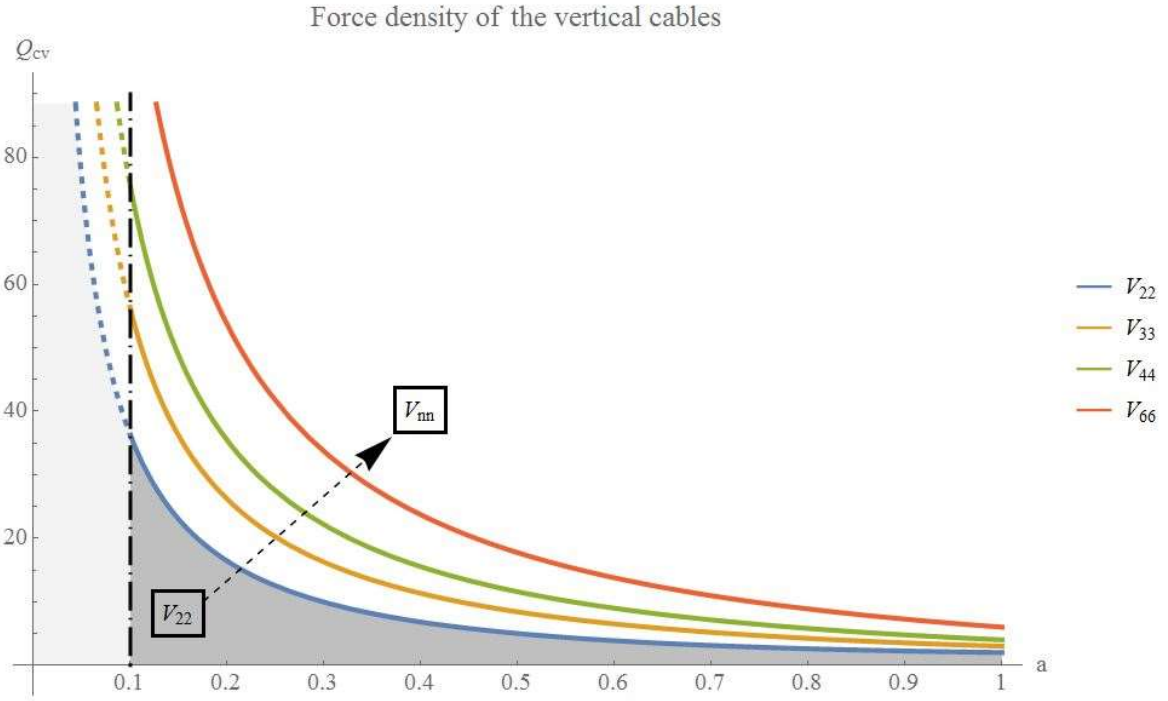

Fig.21 Variation of force densities of the vertical cables of Variant III.

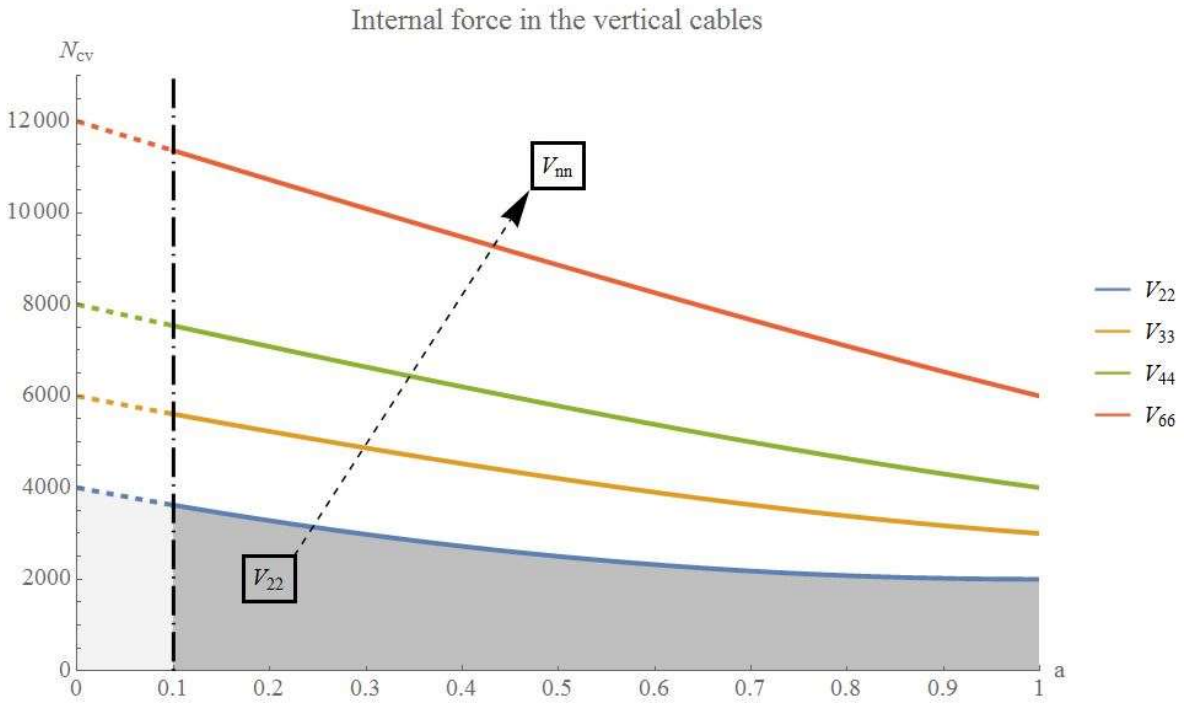

Fig.22 Variation of internal forces in the vertical cables of Variant III.

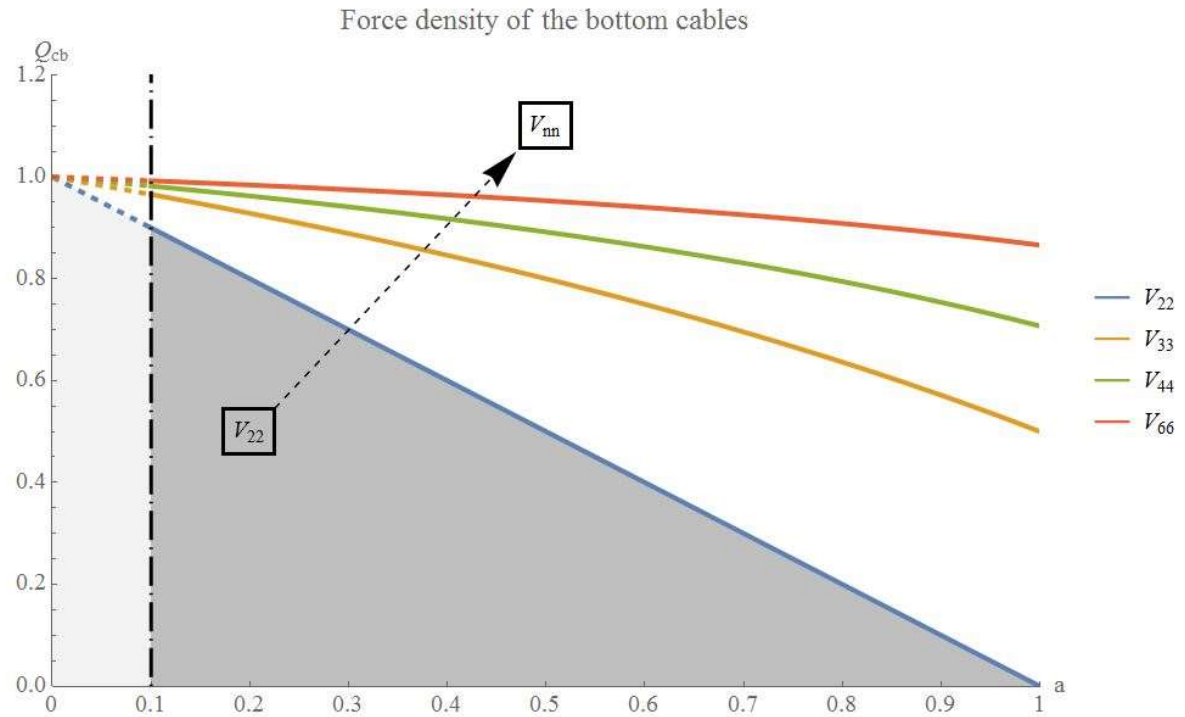

Fig.23 Variation of force densities of the bottom cables of Variant III.

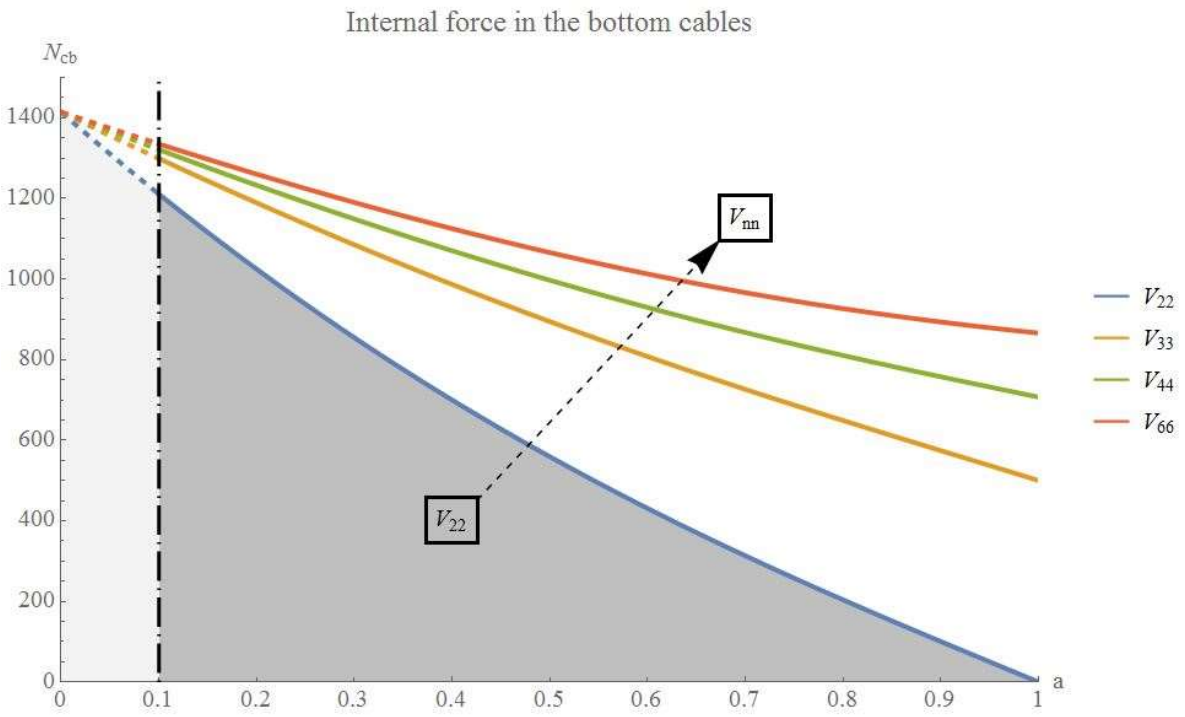

Fig.24 Variation of internal forces in the bottom cables of Variant III.

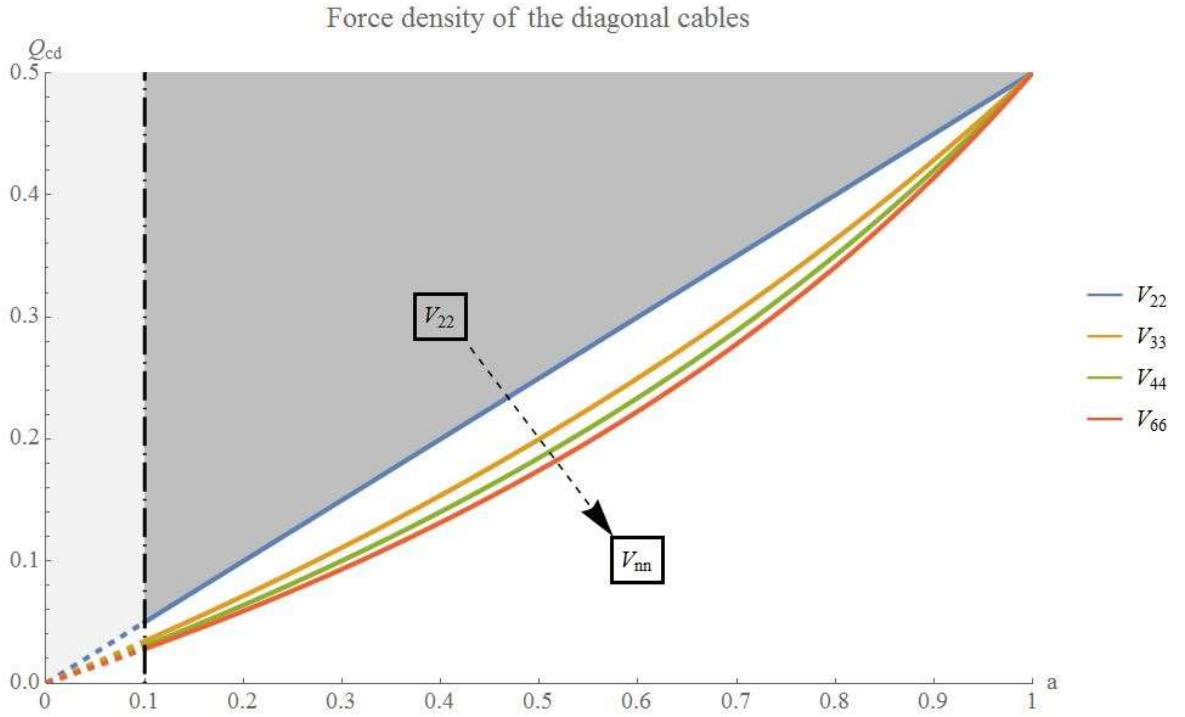

Fig.25 Variation of force densities in the diagonal cables of Variant III.

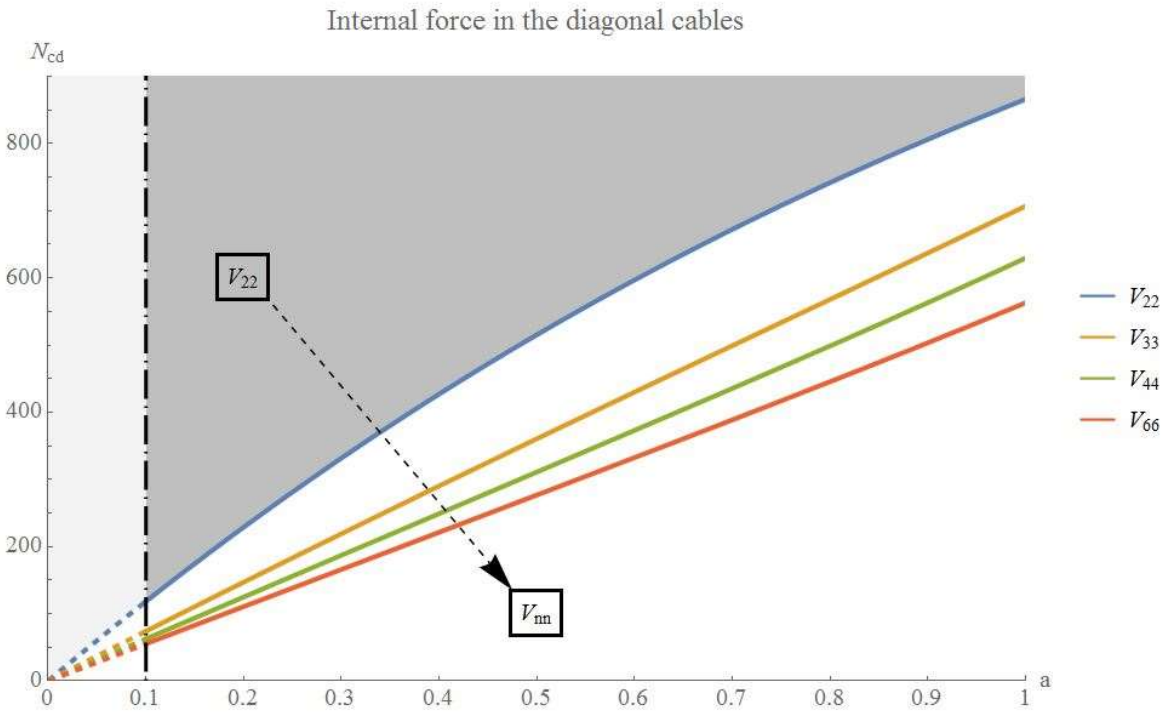

Fig.26 Variation of internal forces in the diagonal cables of Variant III.

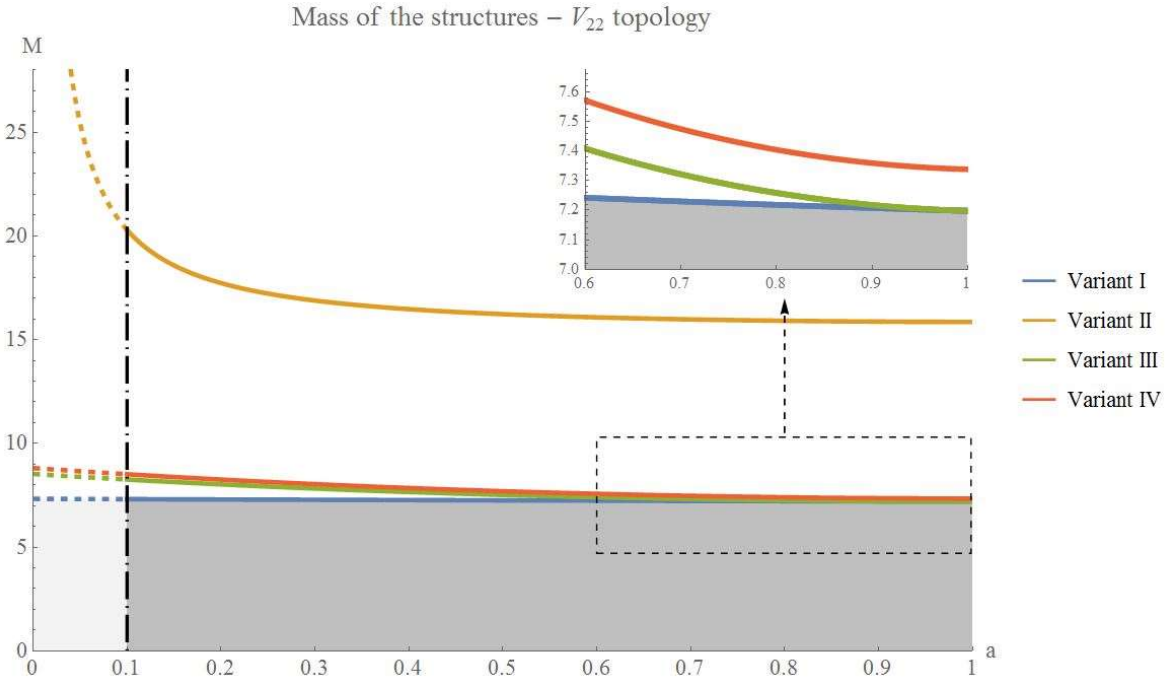

Fig.27 Comparison of masses of V_{22}-Expander topology.

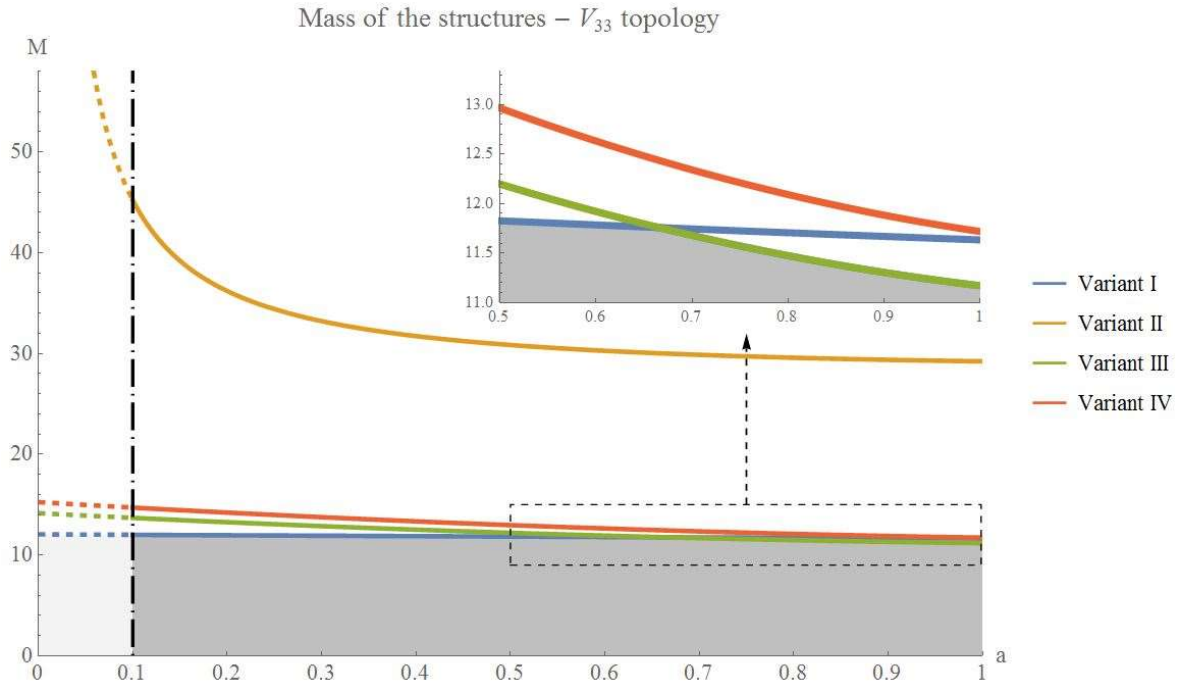

Fig.28 Comparison of masses of V_{33}-Expander topology.

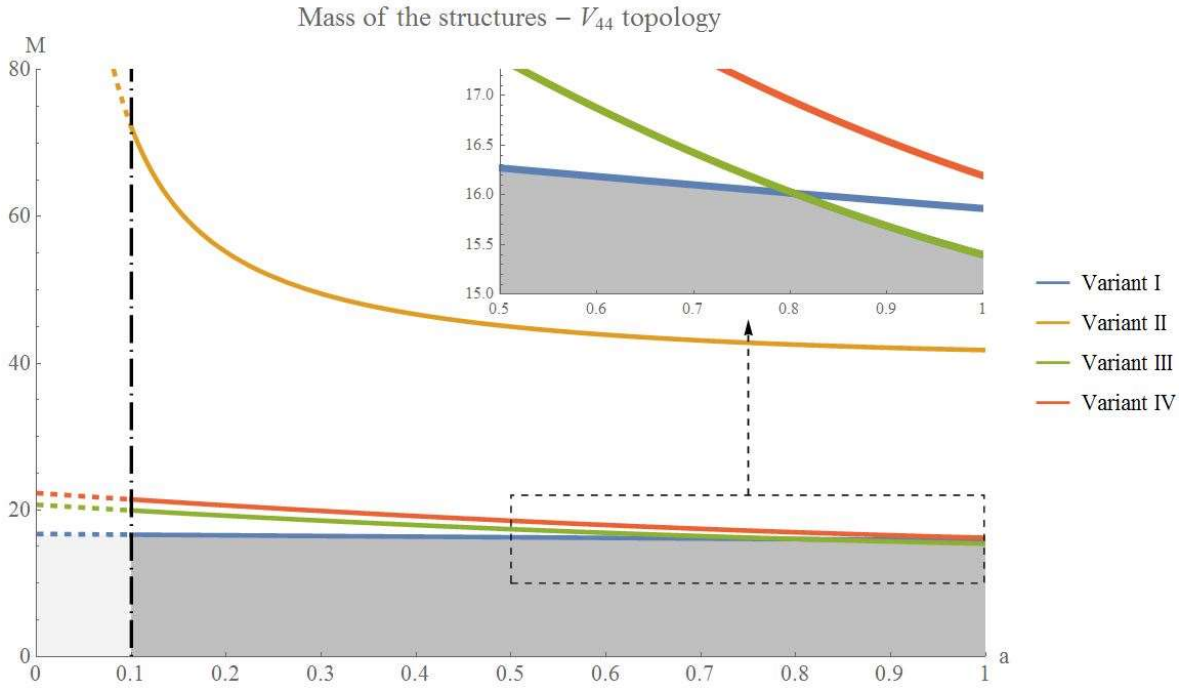

Fig.29 Comparison of masses of V_{44}-Expander topology.

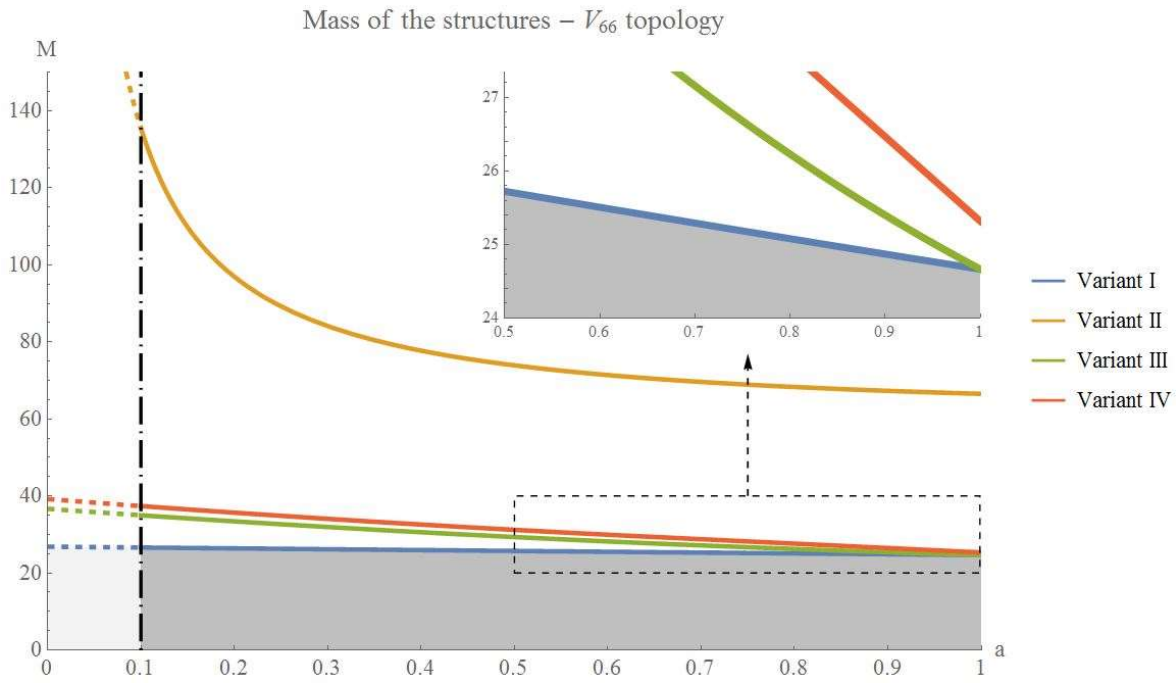

Fig.30 Comparison of masses of V_{66}-Expander topology.